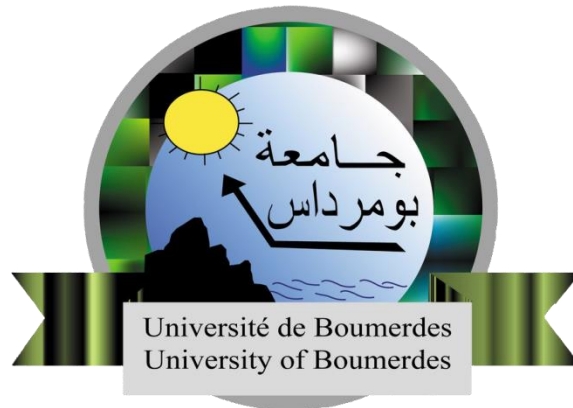


People's Democratic Republic of Algeria
Ministry of Higher Education and Scientific Research
University M'Hamed BOUGARA - Boumerdes



Institute of Electrical and Electronic Engineering
Department of Electronics

Final Year Project Report Presented in Partial Fulfillment of the
Requirements for the Degree of

MASTER

In Power Engineering
Option: Power Engineering

Title

**Design and implementation of PV panel
characterization platform**

Presented by:

- Habes Ahmed**
- Amara Ayoub**

Supervisor:

Pr. Bentarzi Hamid

Abstract

Solar power contribution in producing energy has been increasing rapidly due to the negative impact of rising carbon emissions. Considerable growth of photovoltaic technology installations have been noticed around the world. However, this technology suffers major concerns regarding the efficiency and reliability of system generation. Solar panels' lifespan and efficiency decline over time due to the environment conditions, thereby affecting its main parameters. Weather factors like irradiance and temperature have a direct impact on the overall generation system efficiency and its functionality period. Many attempts have been made in order to interpret the electrical behavior of solar panels module to observe the performance under natural conditions. For monitoring these weather conditions that may affect the main parameters of PV panel, we have developed a new platform frame work using Labview, Ardouino and MOSFET to obtain the current-voltage (I-V) and P-V curves automatically. This platform aids to characterize quickly a solar panel with high accuracy and precision in measurement of its dynamic parameters. The new developed platform uses PC associated with the Arduino to acquire the values of current and voltage from the solar panel under test and store the data for the objective of full analysis of its characteristics under different environmental conditions.

Dedication

This work is dedicated to all of the people who have walked with us on our journey to success in this educational and academic journey. We would like to thank our parents, who played an important role in this course; however, thank you is insufficient to repay their kindness because they did everything they could to make the process as simple as possible for us. We would also like to express our heartfelt gratitude to our brothers, sisters, friends, and family members who have been a source of inspiration for our dreams and goals.

Acknowledgment

Unquestionably, all praise is to Allah for blessing us the potentiality and strength to finish this modest work.

Certainly, all our gratitude and thankfulness go to our beloved supervisor **Pr. Bentarzi Hamid** . We should express our appreciation to him for sincere help and giving comments to guide us. We can never repay his patience in leading us throughout the work.

We would like to thank **Mr. Hanniche Youcef** for his kindness and assistance in completing this work.

Special thanks go to our family and friends for believing in us and encouraging us to keep our enthusiasm along the journey.

Table of Contents

Abstract	
Dedication	
Acknowledgements	
Table of Contents	
List of abbreviations	
List of symbols	
List of figures	
List of tables	
Chapter 1: General Introduction.....	1
1.1 Generalities.....	2
1.2 Motivation.....	2
1.3 Objectives.....	2
1.4 Outlines.....	3
Chapter 2: Photovoltaic Systems.....	4
2.1 Introduction.....	5
2.2 Photovoltaic cells.....	5
2.2.1 Solar Cell Overview.....	5
2.2.1.1 Features of Solar Cells.....	5
2.2.2 Photovoltaic Effect	6
2.2.3 Working principle of Solar Cells.....	6
2.2.4 Main PV Cell Types.....	7
2.2.4.1 Single-Crystalline Silicon.....	8
2.2.4.2 Polycrystalline or Multi-crystalline Silicon.....	8
2.2.4.3 Thin Film.....	8
2.3 module and PV array.....	9
2.4 PV cell modeling.....	9
2.4.1 Single diode model.....	9
2.4.2 Double diode model.....	11
2.5 IV Characteristics of a Solar Cell	11
2.5.1 Its parameters.....	12
2.6 Effect of irradiance and temperature on I–V Characteristic of a Solar Panel.....	13

2.7 Conclusion.....	14
Chapter 3: Software and hardware.....	15
3.1 Introduction.....	16
3.2 Software	16
3.2.1 The Labview Environment.....	16
3.2.2 Virtual Instrument.....	16
3.2.2.1 Front Panel	16
3.2.2.2 Block Diagram.....	17
3.2.3 Tools.....	18
3.2.4 Palettes.....	18
3.2.4.1 Tool Palatte.....	19
3.2.4.2 Control Palette.....	19
3.2.4.3 Function Palette.....	22
3.2.5 Labview Interface for Arduino.....	23
3.3 Hardware.....	24
3.3.1 PV Module STP050D-12/MEA.....	24
3.3.2 Microcontroller Arduino	25
3.3.3 MOSFET.....	26
3.3.4 Temperature Sensor.....	27
3.3.5 Current Sensor	27
3.3.6 Voltage Measurement.....	28
3.3.7 Further components.....	28
3.4 Conclusion.....	30
Chapter 4: Implementation and Results.....	31
4.1 Introduction.....	32
4.2 General block diagram.....	32
4.3 Implementation.....	32
4.3.1 Software part.....	32
4.3.2 Hardware part.....	38
4.3.3 Principle of Operation.....	39
4.4 Test results and discussion.....	40
4.4.1 First test.....	40
4.4.2 Second Test (high temperature and high irradiance).....	42

4.4.3 Third Test (Effect of irradiance).....	43
4.5 Conclusion.....	44
Chapter 5: General Conclusion.....	45
General Conclusion.....	46
Bibliography.....	48
Appendix A	

List of abbreviations

Abbreviation	Definition
PV	Photo-Voltaic
DC	Direct Current
FF	Fill Factor
MP	Maximum Power
SD	Single Diode
DD	Double Diode
STC	Standard Test Conditions
LabVIEW	Laboratory Virtual Instrumentation Engineering Workbench
VI	virtual instrument
FP	Front Panel
BD	Block Diagram
LED	light-emitting diode
LIFA	LabVIEW Interface for Arduino
VIPM	virtual instrument package manager
IDE	integrated development environment
PWM	Pulse width modulation
ICSP	In-Circuit Serial Programming
USB	universal serial bus
MOSFET	Metal Oxide Semiconductor Field Effect Transistor
FET	Field Effect Transistor
GND	Ground
GWO	Grey Wolf Optimization
ODM	One Diode Model

List of Symbols

Symbol	Description	Unit
V	Voltage	V
I	Current	A
T	Temperature	K
P	Power	W
η	Efficiency	-
AM	Air mass	-
G	Solar irradiance	W/m ²
A	Area	m ²

List of Figures

Figure 2.1 Solar Cell.....	5
Figure 2.2 Photovoltaic device working process.....	7
Figure 2.3 <i>Solar Panels</i>	8
Figure 2.4 Photovoltaic configuration.....	9
Figure 2.5 Single diode model.....	10
Figure 2.6 Double diode model.....	11
Figure 2.7 I-V characteristic curve.....	12
Figure 2.8 Effect of irradiance on I–V characteristics.....	13
Figure 2.9 Effect of temperature on I–V characteristics.....	14
Figure 3.1 Front panel window.....	17
Figure 3.2 Block diagram window.....	18
Figure 3.3 Toolbar front panel.....	18
Figure 3.4 Toolbar block diagram.....	18
Figure 3.5 Tool palette.....	19
Figure 3.6 Controls palette.....	20
Figure 3.7 Numeric sub palette.....	20
Figure 3.8 Boolean sub palette.....	21
Figure 3.9 String and Path sub palette.....	21
Figure 3.10 Function palette.....	22
Figure 3.11 For loop.....	22
Figure 3.12 While loop.....	23
Figure 3.13 Arduino palette in LabVIEW.....	24
Figure 3.14 STP050D12/MEA.....	25
Figure 3.15 Arduino Uno Pins.....	26
Figure 3.16 MOSFET IRF740.....	26
Figure 3.17 LM35 temperature sensor.....	27
Figure 3.18 ACS712-05BT Hall Effect current sensor.....	28
Figure 3.19 Circuit for voltage measurement.....	28
Figure 3.20 Resistor.....	29
Figure 3.21 Capacitor.....	29
Figure 3.22 KIA234P.....	29
Figure 3.22 Power resistor.....	29

Figure 4.1 General block diagram of I-V characterization platform.....	32
Figure 4.2 The Block Diagram.....	33
Figure 4.3 PWM write pin.....	34
Figure 4.4 LabView Temp Measurement Block.....	34
Figure 4.5 LabView Voltage Measurement Block.....	35
Figure 4.6 LabView Current Measurement Block.....	35
Figure 4.7 The front panel.....	36
Figure 4.8 Schematic diagram.....	38
Figure 4.9 Circuit Implementation.....	39
Figure 4.10 Test under conditions Temp 45.57°	40
Figure 4.11 Simulation I-V and P-V characteristics.....	41
Figure 4.12 High temperature test (sunny day).....	42
Figure 4.13 Low irradiance test (cloudy day).....	43

List of tables

Table 1	The electrical characteristics of STP050D-12/MEA.....	24
Table 2	Comparison of Experimental and simulation model values.....	41

Chapter 1

General Introduction

1.1 Generalities

The conventional energy sources are no longer sufficient to meet up the increasing demands for power and electricity. The population growth over the past half century led to an accelerating increase of energy consumption which has negatively affected the environment deterioration and increased carbon emission .It is therefore, essential to plan for the future needs of energy moving toward the use of more ensuring renewable energy to cover the rising demands.[1]

The solar energy as a natural replenished source has always been of great appreciation due to the depletion of the conventional sources. Oil, gas and other fossil fuels have exhausted the earth and are likely to be vanished soon, whereas others would be lasting for a long time [1]. Consequently, the photovoltaic is regarded as reassuring tool to maintain an ongoing reservoir of energy on earth; it provides a clean and sustainable energy, that will allow being less dependent on conventional sources. PV installation are becoming progressively wide spread and proven simple operational set, as the technology allows direct conversion of sunlight into electricity .Thus, solar irradiance and temperature are the leading criteria in the electricity generation.

1.2 Motivation

Solar cell technology has been developing rapidly, leading to great improvements in the production of energy. Accordingly, this has constituted a ground for a game changing technology to harvest the sun's energy. In the light of this, studies have become even more interested in PV technology attempting to upgrade the exploitation of the solar panels based on the I-V characteristic curve of the PV systems.

It is essential to analyze power system reliability to narrow the limit of interruption caused by the environment conditions which in turn will affect solar panels longevity .Based on the forgoing, this research tries to evaluate the performance of PV panels by designing and plotting (I-V) characteristics curve. This leads to an automatic lecture and a direct storage of parameters at any fixed time frame.

1.3 Objectives

Consequently, this project tries to shed light on the acquisition of the PV panel's dynamic parameters and automatic plotting of the curves. It attempts to maintain the full exploitation of the solar panels characteristics in front of the changing environmental

parameters. Above all, their overall aim is to design and implement a platform can acquire all these dynamic parameters of PV panels under different conditions. In other words, this project can save all the real time data for analysis purpose.

1.4 Outlines

This report is divided into five main chapters. After general introduction presented in this chapter, chapter two deals with the PV cell construction description and its different types, then the PV cell characteristic. Besides, this chapter talks about the PV cell modeling and the main parameters. In chapter three, a Real-time characterization platform software as well as its hardware components that may be needed for its implementation will be introduced starting with the graphical instrumentation program (Labview) used to minimize physical components. Labview as software tool will take place in measurement and control part in this platform. The control part will be done using transistor programmed by Labview program that may be presented in chapter four. Besides, in this chapter, the complete system implementation with tests will be discussed. The implementation of the measurement circuit as well as the Labview program are explained. Finally, the report ends up by a conclusion as chapter five.

Chapter 2

Photovoltaic System

2.1 Introduction:

Photovoltaic systems can be defined as a source of renewable energy that transforms sunlight to electrical energy. It contains two basic portions: stand-alone and grid connected PV system [2]. Moreover, Solar cells are simple semiconductor devices. Yet, they are the most prominent component of this revolutionary technology. Besides, solar cells can be gathered to create modules connected in series or in parallel to generate an array in order to increase the production of power [3]. Finally, other details will be introduced and discussed later in this chapter such as; its structure, operation, and some affecting factors.

2.2 Photovoltaic cells

2.2.1 Solar Cell Overview

A solar cell can be termed as electronic device that has the ability to convert the solar energy directly into electricity without any changes in the place of its parts through the contribution of photovoltaic effect. A Solar cell is also known Photovoltaic (PV) Cell as shown in figure 2.1. [4]



Figure 2.1 Solar Cell.

2.2.1.1 Features of Solar Cells

- It is a no moving and solid device.
- “Photo” is defined as Light and “voltaic” indicates generating electricity.

- It is an electronic device composed of semiconductor substances like silicon.
- In solar cells, energy of light is directly converted into Direct Current (DC).
- In solar cells, the heat of light is not utilized to produce electrical energy.
- Many factors, like shading on cells, irradiance, temperature act, exert an influence on the efficiency of solar cell.
- In 2014, the multiple junction cells are used to reach the highest 44.7% efficiency.[4]

2.2.2 Photovoltaic Effect

The photovoltaic effect is regarded as the property that enables a photovoltaic cell produces a voltage and electric current once it is subjected to sunlight.

The usefulness of the solar panels is determined by this effect. This is due to the way the cells in the panel transform the light of the sun to electrical energy. The scientist called Edmond Becquerel who has brought to light the photovoltaic effect in 1839. He observed that the increase of the voltage is the result of the cell's silver plates' exposure to sunlight. This has been detected when experimenting with wet cells [5].

2.2.3 Working principle

In the solar cells, it takes place an effect called the photovoltaic effect. The main parts of the solar cell are two distinctive kinds of the semiconductor: - a p-type and an n-type. These semiconductor types are combined for the sake of creating a p-n junction. As soon as the two types of semiconductors are joined, an electronic field is produced. Similarly, the electrons' movements to the positive p-side along with the holes' movements to the negative n-side are also considered the outcome of this junction. This results in a field which in turn provokes the movements of negatively charged particles (electrons).

Light consists of tight bundles of electromagnetic radiation or energy referred to as photons. The photovoltaic cell as the main component of the solar panels has the ability to absorb these photons. The transmission of the photons' energy to an atom of the semiconducting material in the p-n junction is established each time light of the appropriate wavelength is incident on photovoltaic cells. This allows the jumping of the electrons to a superior energy level termed as the conduction band. This leads to the creation of hole in the valence band that allows electrons to jump up from. The added energy that generates this

movement of electrons triggers two different charge carries or an electron-hole pair as shown in Figure 2.2.[5]

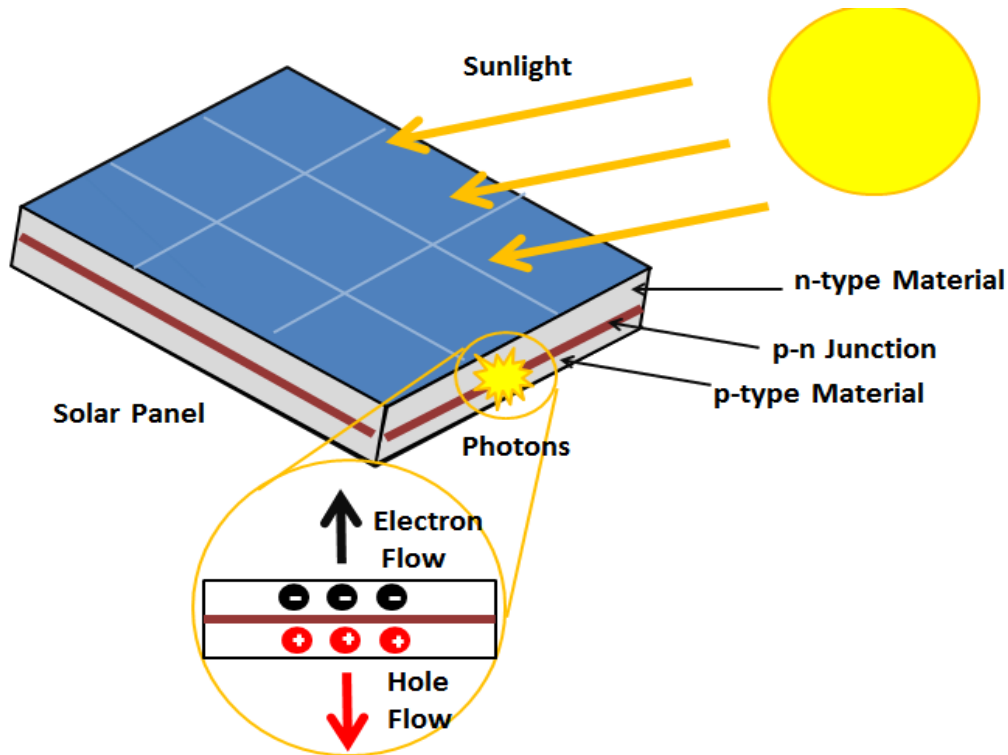


Figure 2.2 Photovoltaic device working process.

The unexcited electrons block whenever these electrons keep the semiconductor material. This is associated with the formation of bonds with the surrounding atoms. Though, these excited electrons move freely through the material in the conduction band. The electric field that emerges from the p-n junction introduces the expected movements of electrons and holes in opposite directions. The free electrons have tendency to travel to the n-side rather than attracting to the p-side. In the PV cell, an electric current is generated due to the movements of the electrons. Whenever the movement of electrons occurs, a hole is left. However, the movement of these holes is possible only in the opposite direction to the p-side. Therefore, this operation produces a difference in potential in the cell. [5]

2.2.4 Main PV Cell Types

The silicon is considered as the material that is largely utilized in the photovoltaic cells manufacturing. There is many types of PV cells, however; the most important ones are the following:

2.2.4.1 Single-Crystalline Silicon

The primary substance is mono-crystalline silicon. The process of making it includes the silicon's purification, melting, and its crystallization into ingots. In order to make separated cells, these ingots are divided into thin wafers. This sunlight conversion technology can be the most ancient and more high-priced production technology, but, it stills the most effective and widely adopted attainable technology. The efficiency of the cells varies between 17% and 22%. [6]

2.2.4.2 Polycrystalline or Multi-crystalline Silicon

One of the main characteristics of this kind of cells is its large size and its easy formation into the shape of square. These qualities allow the elimination of passive areas between the cells. However, it is characterized by insignificantly less conversion efficiency in comparison with single crystalline. Besides, the charges of the fabrication are lower. The efficiency of the cells is between 11% and 17%. [6]

2.2.4.3 Thin Film

The most crucial difference between Amorphous or thin film silicon and crystalline form cells is the solidity. The arrangement of the silicon atoms in these cells is more chaotic than the other form. The cells' efficiency occurs between 6% and 11%. [6]

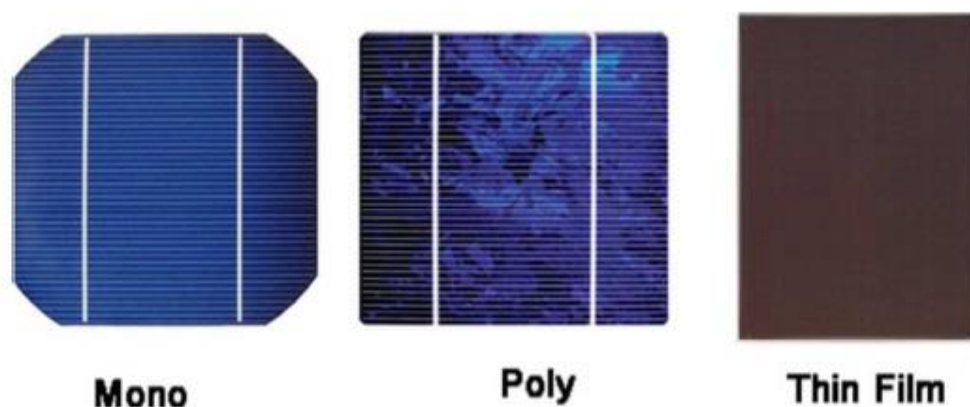


Figure 2.3 Solar Panels.

2.3 PV module and PV array

The solar cell which is a main element of a PV module cannot be implemented alone due to its limited voltage and power supply. A connection of many photovoltaic cells in parallel or series leads to generate more power with high voltage. The connection of cells in series realizes more voltage, while the connection of cells in parallel achieves more generation of current. A solar array or panel can be defined as the assemblage of multiple modules that are linked electrically in series-parallel configuration as shown in figure 2.4. This configuration leads to the generation of the necessary power. [7]

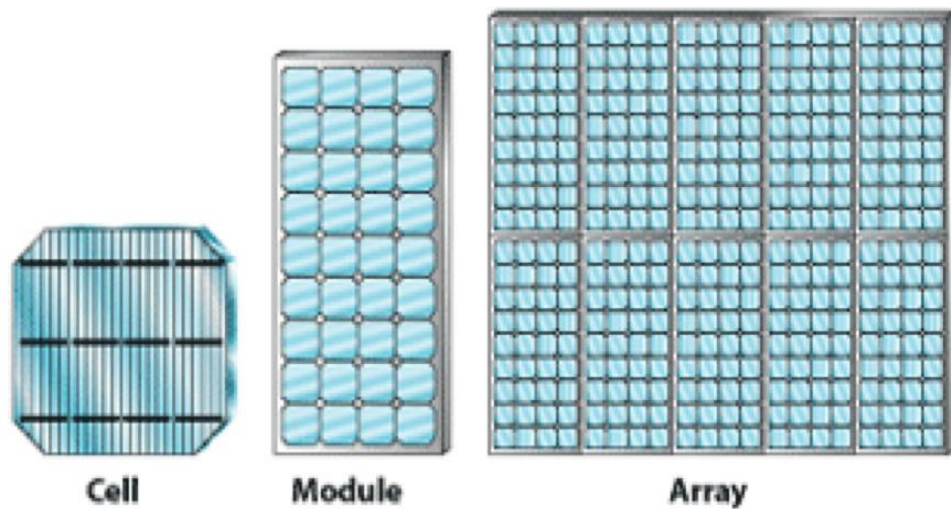


Figure 2.4 Photovoltaic configuration.

2.4 PV cell modeling:

For a deeper understanding the operation of a solar cell, it is necessary to construct an electrically equivalent model. Researchers use a variety of electrical models to describe the physical behaviors of PV cells. Single diode (SD) and double diode (DD) models are the most common used models.

2.4.1 Single Diode Model:

Single Diode Model is an equivalent circuit of a practical PV cell. In many literatures, it is termed as a five parameter model ($R_s, R_p, I_0, I_{ph}, \eta$). It takes into account different properties of solar cell as:

- R_s is introduced to consider the voltage drops and internal losses due to flow of current.
- R_p takes into account the leakage current to the ground when diode is in reverse biased.
- But this model has neglected recombination effect of diode, which is why it is still not the most accurate model [8].

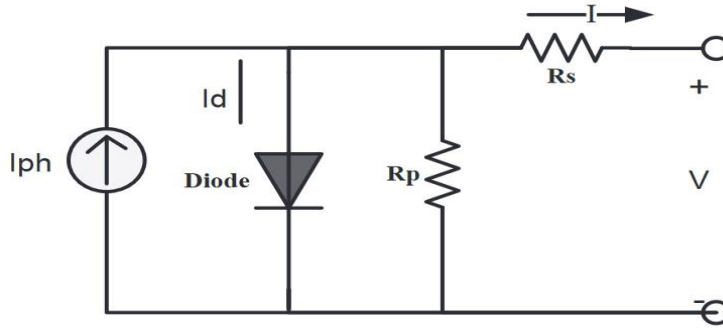


Figure 2.5 single diode model.

According to the schematic of a solar cell equivalent circuit illustrated in Fig.2.5, the output current of a photovoltaic cell is given in equation (2.1)

$$I = I_{ph} - I_d - I_p \quad (2.1)$$

Where I represents the output current, I_{ph} the photo-generated current, I_d the diode current, and I_p the current through the parallel resistor.

From Shockley the diode current is presented as Eq. (2.2), meanwhile the current flows through parallel resistance is written as Eq. (2.3).

$$I_d = I_s \left(e^{\frac{V + R_s I}{a V_t}} - 1 \right) \quad (2.2)$$

$$I_p = \frac{V + R_s I}{R_p} \quad (2.3)$$

Where I_s is the reverse saturation current of the diode. V denotes the terminal voltage, R_s and R_p series and parallel resistors respectively, a is the diode ideal factor. V_t is the junction thermal voltage and is defined by Eq. (2.4).

$$V_t = \frac{T \cdot k}{q} \quad (2.4)$$

Where T indicates the cell temperature in Kelvin, k is the Boltzmann constant ($1.381 \times 10^{-23} \text{ J/K}$), and q is the electron charge ($1.602 \times 10^{-19} \text{ C}$).

By substituting these values in equation (2.1)

$$I = I_{ph} - I_s \left(e^{\frac{V + R_s I}{a V_t}} - 1 \right) - \frac{V + R_s I}{R_p} \quad (2.5)$$

2.4.2 Double Diode Model:

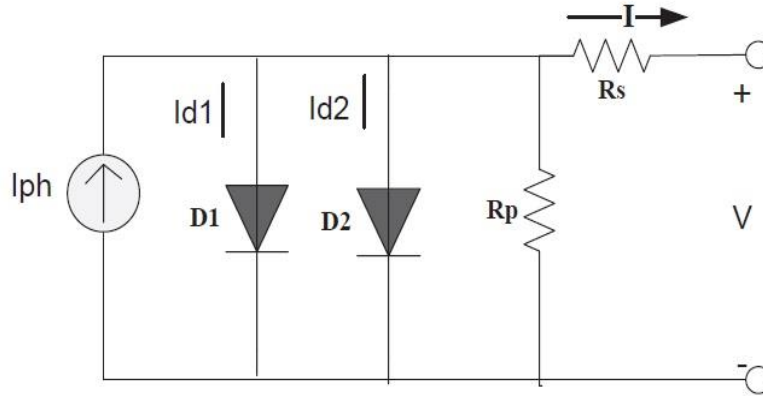


Figure 2.6 Double diode model.

Double Diode Model shown in figure 2.6 is the modified form of single diode model which takes into account the effect of recombination by introducing another diode in parallel.

$$I = I_{ph} - I_{D1} \left(e^{\frac{V + R_s I}{a V_t}} - 1 \right) - I_{D2} \left(e^{\frac{V + R_s I}{a V_t}} - 1 \right) - \frac{V + R_s I}{R_p} \quad (2.6)$$

Taking into account mathematical computation and number of iterations, the advantages of single diode model and two diode models are as follows. The privilege of single diode model is its speed in giving the results due to simplicity in its equation and its accuracy. While, the two diode model provides sharper and more exact characteristics in different weather circumstances along with the calculation of parameters and more extended iterations. [8]

2.5 I-V Characteristics of a Solar Cell

The (I-V) curve of a solar cell is obtained from the voltage, current, and power characteristics of a particular PV cell, array, or module. These features provide data concerning the electrical behavior and its capability to produce power. Bearing in mind that manufacturers provide parameters of PV modules and the (I-V) characteristics in the standard test conditions. These conditions are represented by STC: 1000W/m² of irradiance, 25°C cell temperature and air mass 1.5. [9]

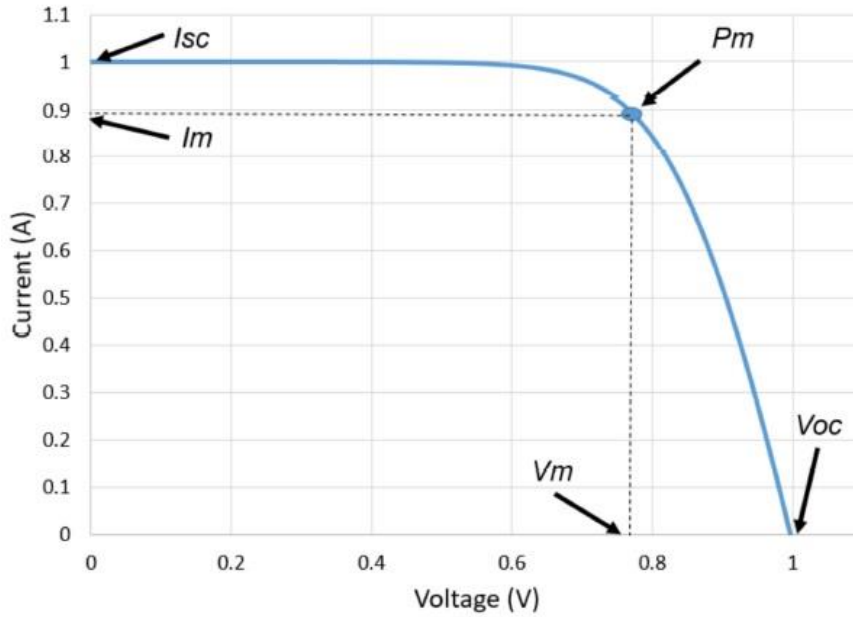


Figure 2.7 I-V characteristic curve.

2.5.1 A PV Cell Parameters

The main parameters that characterize a photovoltaic cell are: [10]

- **Open-Circuit Voltage V_{oc} :** The open circuit voltage of the solar cell is the maximum voltage; its value can be achieved when there is no load and current passing through the cell.
- **Short-Circuit Current I_{sc} :** The short circuit current of the solar cell is the maximum current; its value can be achieved when there is no load and voltage.
- **Maximum power point:** The maximum power point of the solar cell is the maximum power that the solar cell is able to produce in the operating conditions. It is the area of the product of the maximum current I_{mp} and Voltage V_{mp} as shown in the equation (2.7).

$$P_{mp} = V_{mp} * I_{mp} \quad (2.7)$$

- **Fill Factor FF:** FF can be defined as the ratio of the maximum power (MP) generated by the solar cell to the product of the voltage open circuit V_{oc} and the short circuit current I_{sc} .

$$FF = \frac{\text{Power at mpp}}{\text{Theoretical maximum power}} = \frac{V_{mp} \cdot I_{mp}}{V_{oc} \cdot I_{sc}} \quad (2.8)$$

- **Conversion efficiency of the device (η):** The connection of solar cell to an electrical circuit leads to the conversion and the collection a percentage of power. This is referred to as Conversion efficiency of the device (η). Besides, the calculation of this term is executed through the use of a ratio of the maximum power point, P_{max} , divided by the input light irradiance (G , in W/m^2) in the standard test conditions (STC) and the surface area of the solar cell (A_c in m^2).

2.6 Effect of irradiance and temperature on I–V Characteristic of a Solar Panel

The solar irradiance on earth ground varies. However, the highest level that can be reached is $1000 W/m^2$. The cloud, the earth movements and many other factors can lead to the decrease of the solar irradiance will automatically cause a reduction in the output current of the solar panel. This is due to the fact that the solar panels are directly proportional to the sun irradiance with insignificant variation on the voltage as illustrated in figure 2.8.

The temperature change provokes a variation in the solar cells performance. This alteration in temperature will impact on the power output produced by the cells. The voltage and the temperature are interrelated. In other words, any rise of temperature will induce the decrease in the voltage as shown in Fig.2.9. [11]

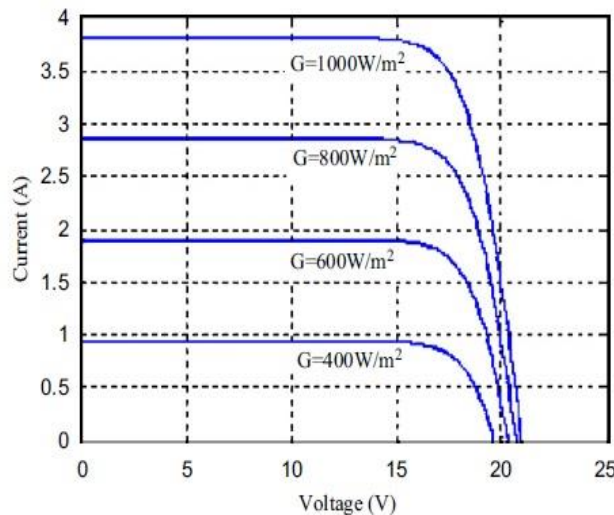


Figure 2.8 Effect of irradiance on I–V characteristics.

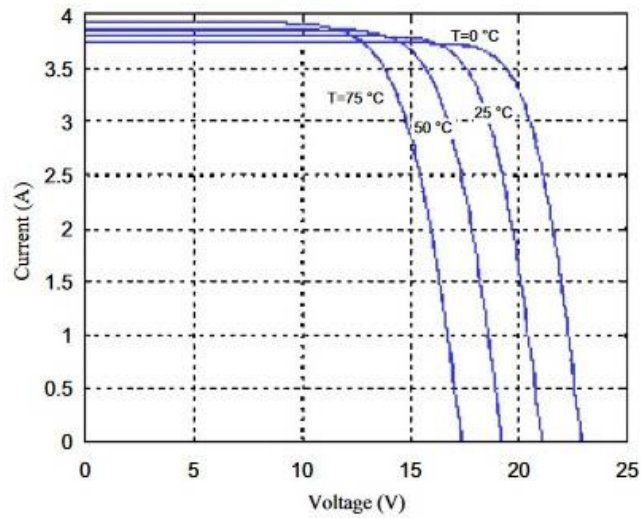


Figure 2.9 Effect of temperature on I–V characteristics.

2.6 Conclusion

To conclude with, this chapter has tackled the PV panels in details .This is to bring to light the concerned project .However, the next chapter will present keystone that will promote a better understanding of the current research. .

Chapter 3

Software and Hardware Components

3.1 Introduction

LabVIEW has been chosen as software development tool to implement this platform. An effort to dig deeper, the chapter will introduce the main Software and Hardware Components needed for Platform Implementation. Starting by an overview of the different components that may be used in the hardware part will be presented. Thus, the embedded system by the integration of both the software and hardware is attended to the most advantageous execution of the project.

3.2 Software

3.2.1 Labview

LabVIEW (short for Laboratory Virtual Instrumentation Engineering Workbench) is a platform and development environment for a visual programming language from National Instruments. The graphical language is named "G".. LabVIEW graphical programs are called virtual instruments (VIs). LabVIEW is commonly used for data acquisition, instrument control, and industrial automation on a variety of platforms including Microsoft Windows, various flavors of UNIX, Linux, and Mac OS X...[12].

3.2.2 The LabVIEW Environment

Another expression for LabVIEW programs is **Virtual Instruments**, or VIs. VIs is the critical part of LabVIEW. In other words, the VIs is what makes LabVIEW distinguishable from the rest text-dependent development environment .Additionally, its main two elements are a Front Panel (FP), and a Block Diagram (BD) [13].

3.2.2.1 Front Panel

The front panel is recognized as the interface that the user interact through .Additionally, it contains the indicators and their controls .These two elements are regarded as the interactional input and output terminals of the VI. On one hand, graphs, LEDs, and other displays present the indicators .On the other hand, knobs, push, buttons, dials, and other input devices introduce make known the controls. The prominent functions of the controls are the stimulation of instrument input device together with the supplying of data to block diagram of

the VI. Still, the role of indicators is unlike .The indicators trigger the instrument output devices and exhibit data acquired or produced by the block diagram [13].

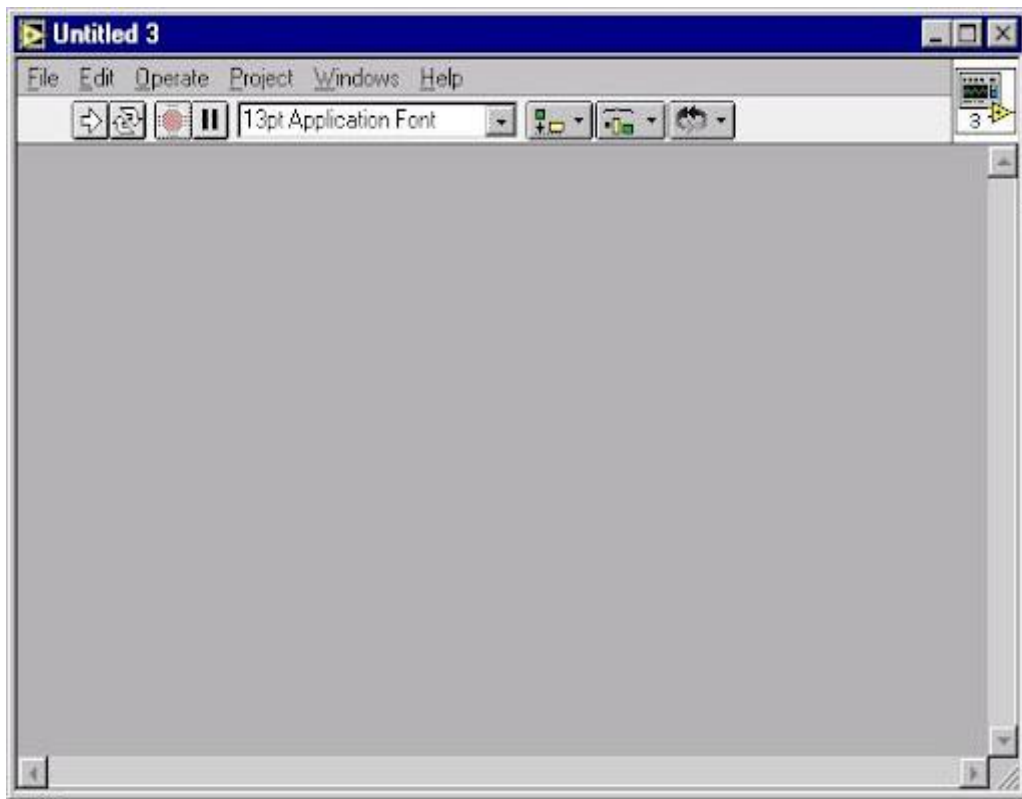


Figure 3.1 Front panel window.

3.2.2.2 Block Diagram

The crucial task of the block diagram is to create a link or connection between the input and the output, along with multiple functional components. After the construction of the front panel, the code is implemented through graphical representations of functions objects. As an effort of taking control over the front panel objects, the code addition is prominent. Also, it is apparent that the block diagram comprises the code of the graphical source. On the block diagram, the objects of the front panels display as terminals. Meanwhile, terminals, subVIs, functions, constants, structures, and wires are considered to be the objects of the block diagram .The crucial objective is the data transmission in accordance with the rest of the block diagram objects [13].

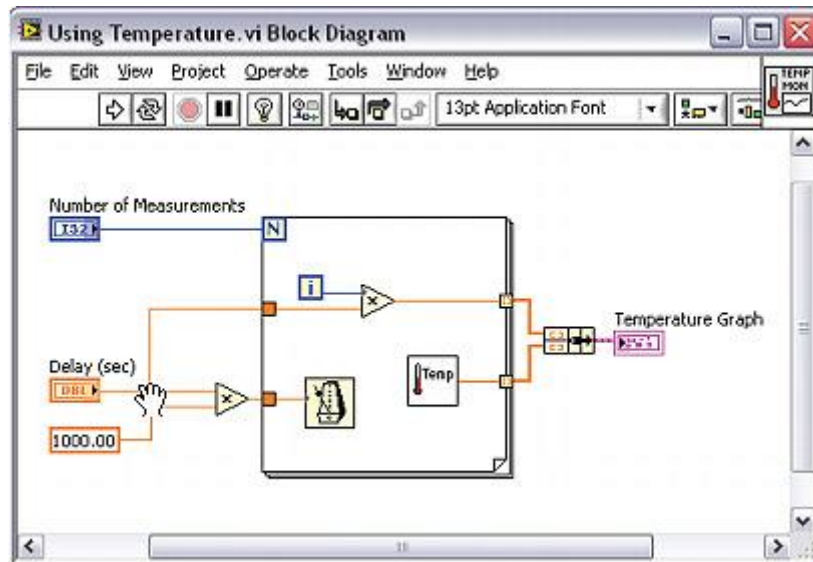


Figure 3.2 Block diagram window.

3.2.3 Tools

Toolbars provide access to program's execution and presentation of tools.

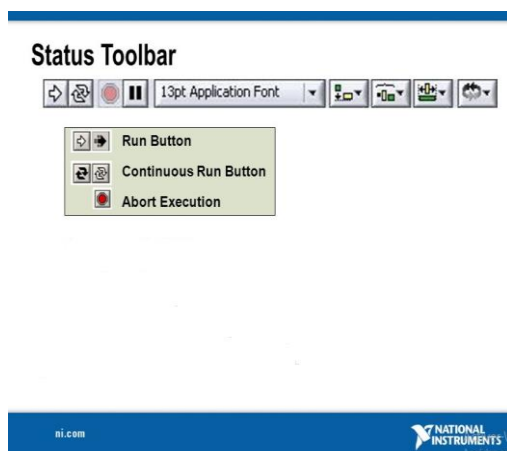


Figure 3.3 Toolbar front panel.

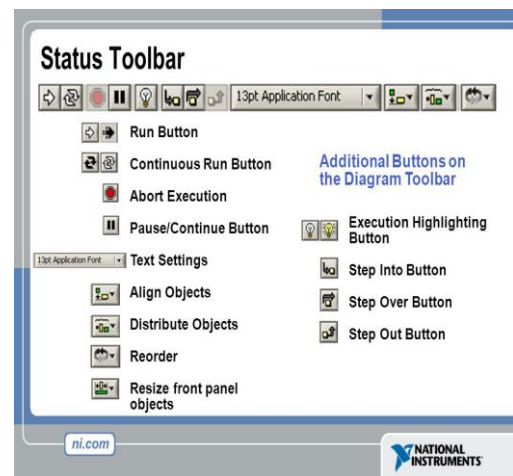


Figure 3.4 Toolbar block diagram.

3.2.4 Palettes

LabVIEW palettes offer a variety of tools. These tools permit the creation and the edition of both the front and the back face of the diagram. There are three types of palettes: [14]

3.2.4.1 Tool Palette

The particularity of the tools palettes is its availability on the block diagram and the front panel simultaneously. The specific operating mode of the mouse cursor is seen as the suitable definition of a tool. In the Tools palette, the cursor refers to the icon of the chosen tool. Moreover, tools are integrated for the operation and the modification of both the block diagram objects and the front panels

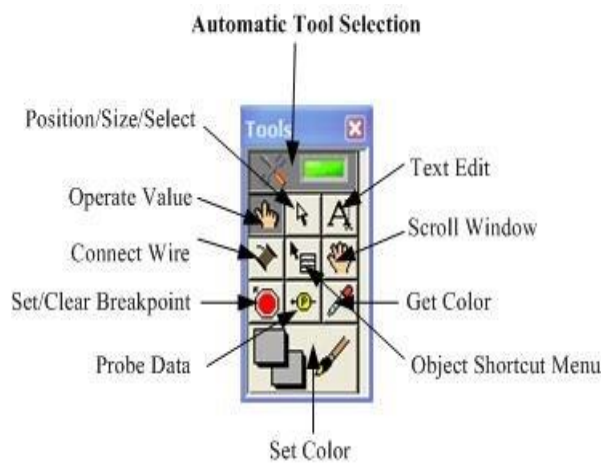


Figure 3.5 Tool palette.

3.2.4.2 Control Palette

The Controls palette has only one access on the front panel. A click on the sub palette icon changes the whole palette into the selected sub palette. The only way to access an object on the palettes is to click on the object and move it whether to the front panel or the block diagram. The Controls palette embodies both the indicators and the controls used for the building of the front panel.

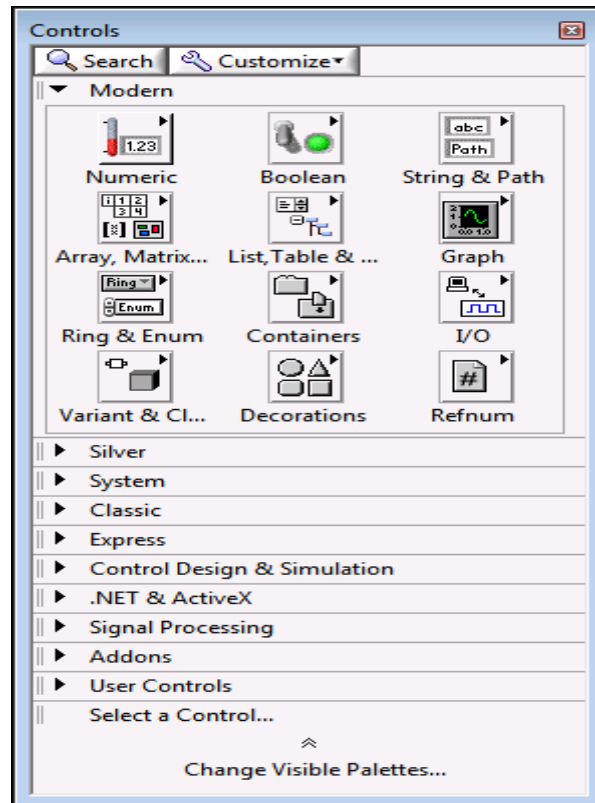


Figure 3.6 Controls palette.

The Controls palettes include sub palettes of objects that are used for the purpose of creating a VI. The most prevalent Sub Palettes are:

- **Numeric Sub Palette:** “Numerical Control” and “Numerical Indicator” are considered as the most popular objects in the numeric sub palette.

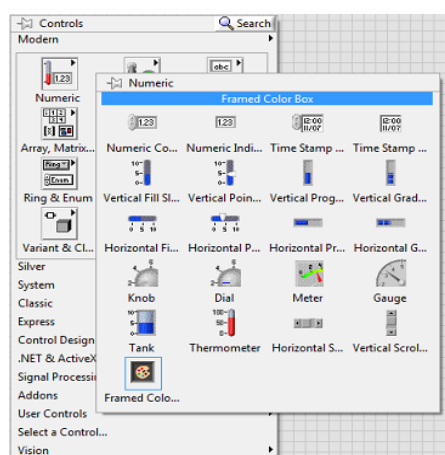


Figure 3.7 Numeric sub palette.

- **Boolean Sub Palette:** This palette has various buttons that can be used.

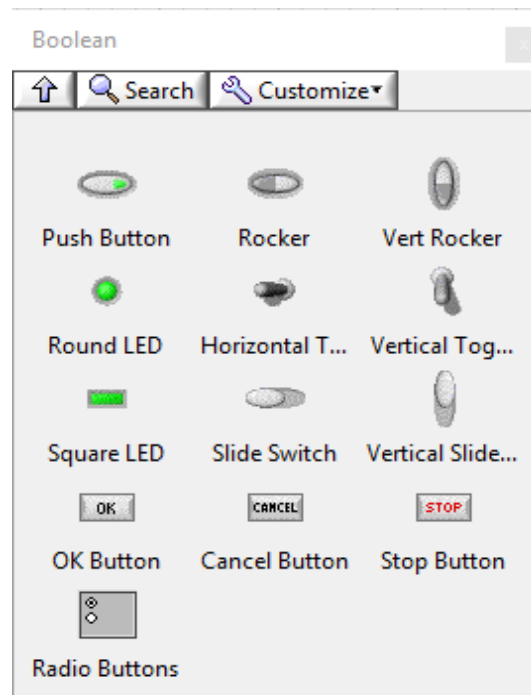


Figure 3.8 Boolean sub palette.

- **String & Path Sub Palette:** This palette contains a plenty of distinctive buttons that can be utilized.

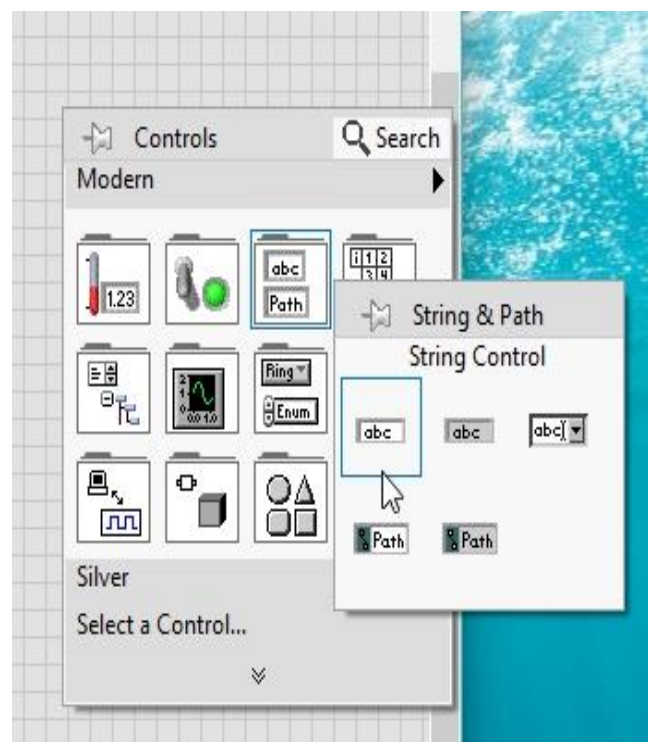


Figure 3.9 String and Path sub palette.

3.2.4.2 Function Palatte

The Functions palette contains function VIs and blocks. However, it can only be accessed through the block diagram

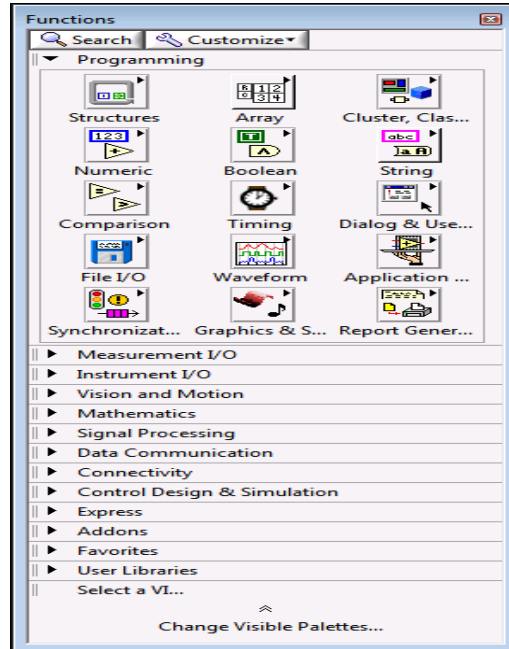


Figure 3.10 Function palette.

Sub palettes of objects are found in the Functions palettes .These sub palettes of objects such as Structures sub palette are used for the creation of a VI. The various Loops are accessible in it. However, this project has adopted the following:

➤ For loop

A For Loop structure is implemented for the execution of repetitions .In Figure 3.11, a For Loop structure is denoted in the displayed border. More precisely, the number of the repetitions the loop executed is introduced as the count terminal **N** while the number of the completed iterations is presented as the iteration terminal **i**. Though, the iteration terminal **i** begins with zero.

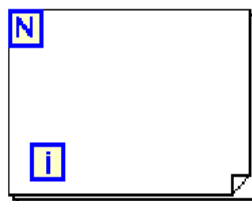




Figure 3.11 For loop.

➤ While loop

A While Loop structure is dependent on a condition in providing repetitions .In Figure 3.12, the true condition allows the conditional terminal  to initiate a stop. In an identical manner to a For Loop, the number of the completed iterations is supplied by the iterations terminal .

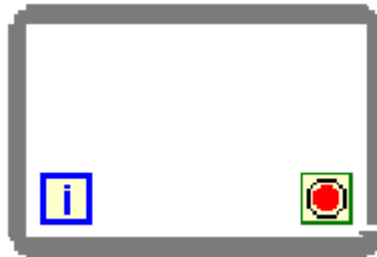


Figure 3.12 While loop.

3.2.5 LabVIEW Interface for Arduino:

In an effort to create an interfacing between LabVIEW with Arduino board, LabVIEW Interface for Arduino (LIFA) is regarded as a LabVIEW toolkit package. All the way back to the beginnings, it is one of National Instrumnet engineer, Sam Kristoff, who brought LIFA toolkit into light. The LIFA toolkit guarantees an easy access to interface for the sake of the Arduino microcontroller platform. Moreover, the LabVIEW Interface for Arduino provides an easy and quick creation of the graphical user interfaces for virtually any elements that is suitable to the Arduino microcontroller. The customization is the end goal of this open source toolkit .This promotes the creation of the custom drivers for the users' sensors. However, the access to the intended open-source toolkit is supported by VIPM. The VIPM stands for VI package manager. Then, the browsing LabVIEW Interface for Arduino is executed and the installation of the package is done .Thus, the availability of the Arduino palette is attained as shown in Figure 3.13 [15].

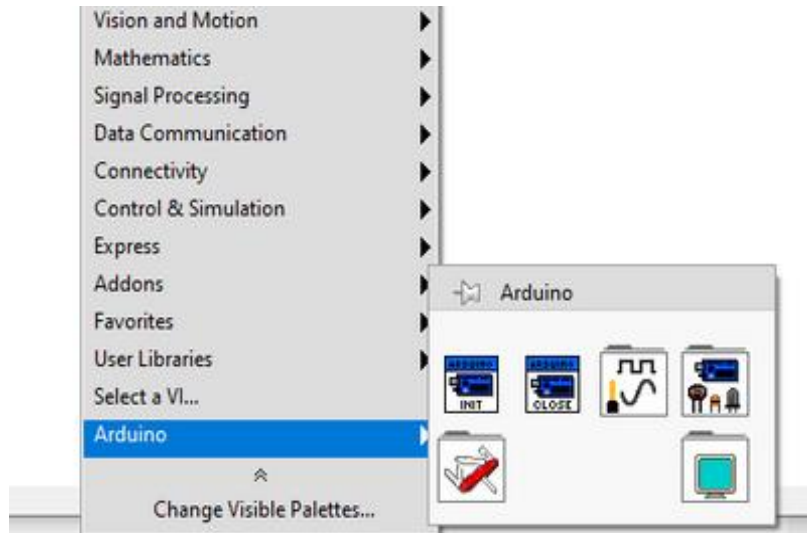


Figure 3.13 Arduino palette in LabVIEW.

3.2 Hardware

3.3.1 PV module STP050D-12/MEA

The electrical characteristics implemented in the experiment of testing PV panel is presented in the table below: [16]

Open-Circuit Voltage (V_{oc})	Optimum Operating Voltage (V_{mp})	Short-Circuit Current (I_{sc})	Optimum Operating Current (I_{mp})	Maximum Power at STC (P_{max})	Operating Temperature	Maximum System Voltage	Maximum Series Fuse Rating	Power Tolerance
21.8V	17.4V	3.13A	2.93A	50 Wp	-40°C to +85°C	715 V DC	10A	±5%

Table 1 The electrical characteristics of STP050D-12/MEA.



Figure 3.14 STP050D-12/MEA.

3.3.2 Microcontroller Arduino

In this project, Arduino UNO has been adopted for multiple reasons. First, it is easy to wire. Second, it can be programmed without difficulty. Finally, it integrates a very complex process of microcontroller chips and electronic circuit design into a cheap, easy-to-program, user-friendly microcontroller package. The Arduino Uno is an open-source microcontroller board based on the ATmega3284. It has 14 digital input/output pins (of which 6 can be used as PWM outputs), 6 analog inputs, a 16 MHz crystal oscillator, a USB connection, a power jack, an ICSP header, and a reset button. [17] For the purpose of coding, Arduino has developed special software termed integrated development environment (IDE). Further; this software aims at providing a full backup to C and C++ programming languages [15].

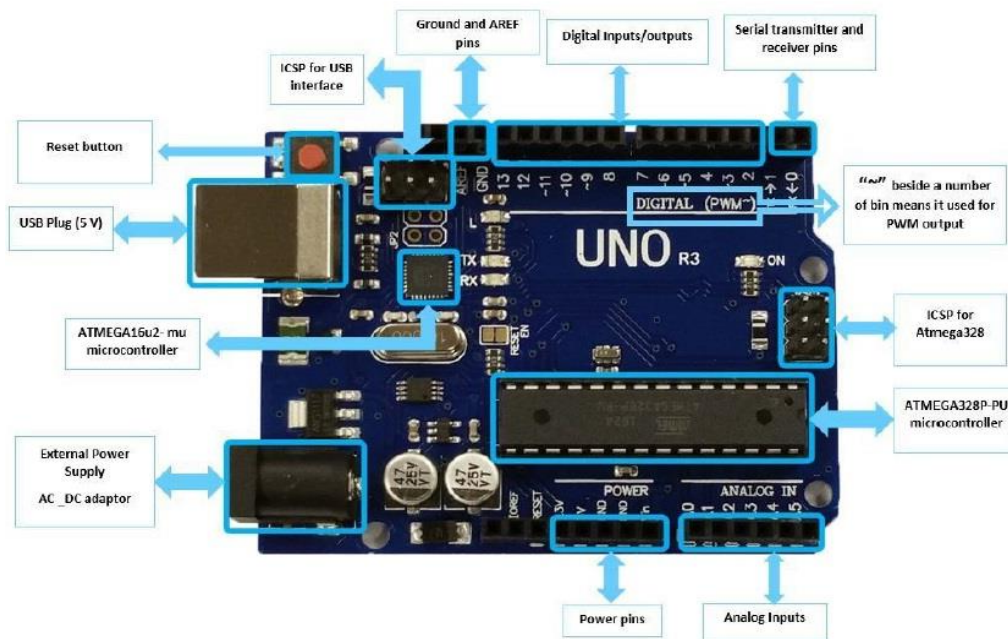


Figure 3.15 Arduino Uno Pins.

3.3.3 MOSFET

MOSFET stands for Metal Oxide Semiconductor Field Effect Transistor. It is a type of FET (Field Effect Transistor). MOSFET has three terminals gate, source and drain. This type of transistor is further classified as p-channel and n-channel. MOSFETs can be seen either as ‘enhancement’ devices, or ‘depletion’ devices. Both enhancement and depletion types are available in N- and P-channel devices [18].

In this project, the MOSFET IRF740 N-channel is used. Where the ‘drain’ and ‘source’ terminals are connected to the load, and the ‘gate’ terminal is the controlling. When the gate signal is high, current can flow from the drain and the source. However, when the gate signal is low, current cannot flow. This MOSFET switch loads up to 400V and could switch the consumption of loads up to 10A. Finally, it can be turned on by providing a gate threshold voltage of 10V across the Gate and Source pin [19].

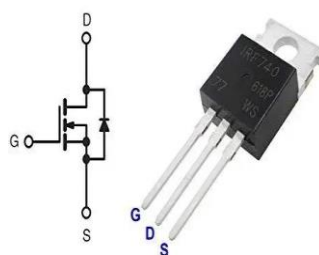


Figure 3.16 MOSFET IRF740.

3.3.4 Temperature sensor

LM35 gains a large popularity in electronic components due to its inexpensiveness, its precise, its reliability as well as its simple manipulation. One of its significant properties is its capacity to function in a range of -55°C to $+150^{\circ}\text{C}$. The voltage provided by LM35 is linearly approximated to the measured temperature that can be expressed in the degree Celsius. More precisely, the increase of temperature by 1°C leads to an increase of the output voltage by 10 mV. [20]

Figure 3.17 shows the pin out of the LM-35 Temperature Sensor:



Figure 3.17 LM35 temperature sensor.

For interpreting and exhibiting the sensor's outcome to any display unit, the output variable is supplied to any analog pin of the Arduino microcontroller .On one hand, the applying supply voltage that enables the working of the sensor (4 - 30 V) is V_{cc} pin .On the other hand, V_{out} pin is used to obtain analog output value from the sensor. Finally, the connection of GND pin to the ground is crucial.

3.3.5 Current sensor

Acs712 can be defined as Hall Effect -Based Linear Current Sensor. The Acs712 feature is its capacity to measure both the Direct and the Altering currents .It is also significant to mention that it exits three types of ASC712 .These three types are relying on the readable current range, $\pm 5\text{A}$, $\pm 20\text{A}$, and $\pm 30\text{A}$. However, this project has adopted the ACS712-05B-T current sensor extending from - 5A to + 5A .The researcher has identified that to obtain a sensitivity of $185\text{mV} / \text{A}$. More importantly, this module takes the measurements of the positive as well as the negative current in the scope of 0-5A.similarly, the input voltage at an Arduino analog pin is considered the same as The output voltage of the

ACS712-05B-T module which varies between 0 and 1023..In the accordance of the remaining circumstances (without any load on the sensor), the V_{cc} is linked to the Arduino, OUT pin on the Sensor outputs 2.5V.Once the addition of the voltage to the load is established ,the voltage increase or decrease is occurred through its sensitivity value. [21]



Figure 3.18 ACS712-05BT Hall Effect current sensor.

3.3.6 Voltage measurement

The use of a voltage divider circuit is required to measure the PV panel's output voltage. This particular circuit construction is based on the use of both of 30 K Ω and 7.5 K Ω resistances. This is clearly demonstrated in figure 5 Moreover, its use is recognized to be the reduction of input voltage up to 5 times in comparison with the initial voltage. This is due to the fact that 5V is considered as the highest input voltage of the Arduino microcontroller.

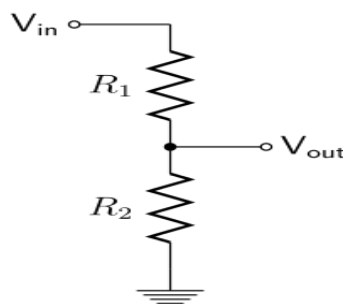


Figure 3.19 Circuit for voltage measurement.

3.3.7 Further Components

- **Resistor**
10k Ω used for filter



Figure 3.20 Resistor.

- **Capacitor**

4.7 μf used for filter



Figure 3.21 capacitor.

- **Operational Amplifier(KIA234P)**

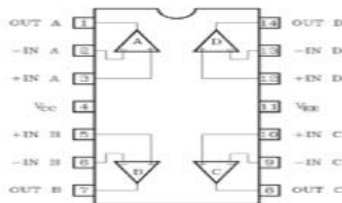


Figure 3.22 KIA234P.

This operation amplifier is used in this project as a voltage follower to make the signal conditioning circuit for the current, voltage and temperature sensors for a protection purposes.

- **Power resistor (0.3 Ω)**



Figure 3.22 Power resistor.

3.3 Conclusion

This chapter has addressed software with LabVIEW as the working environment. Moreover, the indication of hardware with the implementation of various components cannot be ignored.

In the next chapter, a detailed presentation of the I-V characteristics of the PV panel will be discussed.

Chapter 4

Implementation and Results

4.1 Introduction

This chapter discusses the integration of experimental aspects concerning the recorded data about I -V characteristics of the PV panel. The change in these characteristics are determined by the inconstancy of the sun's irradiance and temperature.

4.2 General block diagram

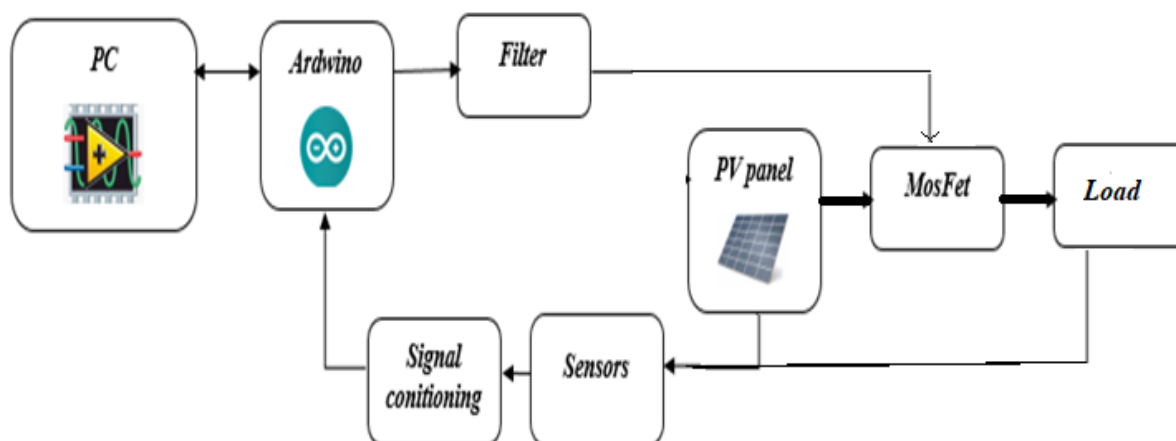


Figure 4.1 General block diagram of I-V characterization platform.

Figure 4.1 represents the general block diagram of the I-V characterization platform. It is mainly composed of a PV panel (STP050D-12 MEA) under test and a host PC for monitoring and processing data, an Arduino UNO card is used for data acquisition and PWM signal generation. Since Arduino can only generate a digital signal, a first-order low pass filter is used to convert the PWM signal with a variable duty cycle to an analog signal to feed the gate terminal of the MOSFET, this latter controls the current and voltage of the PV panel. Using the sensor's data, both I-V and P-V curves can be plotted with their corresponding parameters.

4.3 Implementation

4.3.1 Software Part

To obtain the I-V and P-V curves of the PV panel, LabVIEW software and the Arduino interface toolkit have been used to develop and implement this project. The LabView software programme consists of two main parts, the block diagram which contains the algorithm of this task and the front panel which is the user interface.

i) Block Diagram

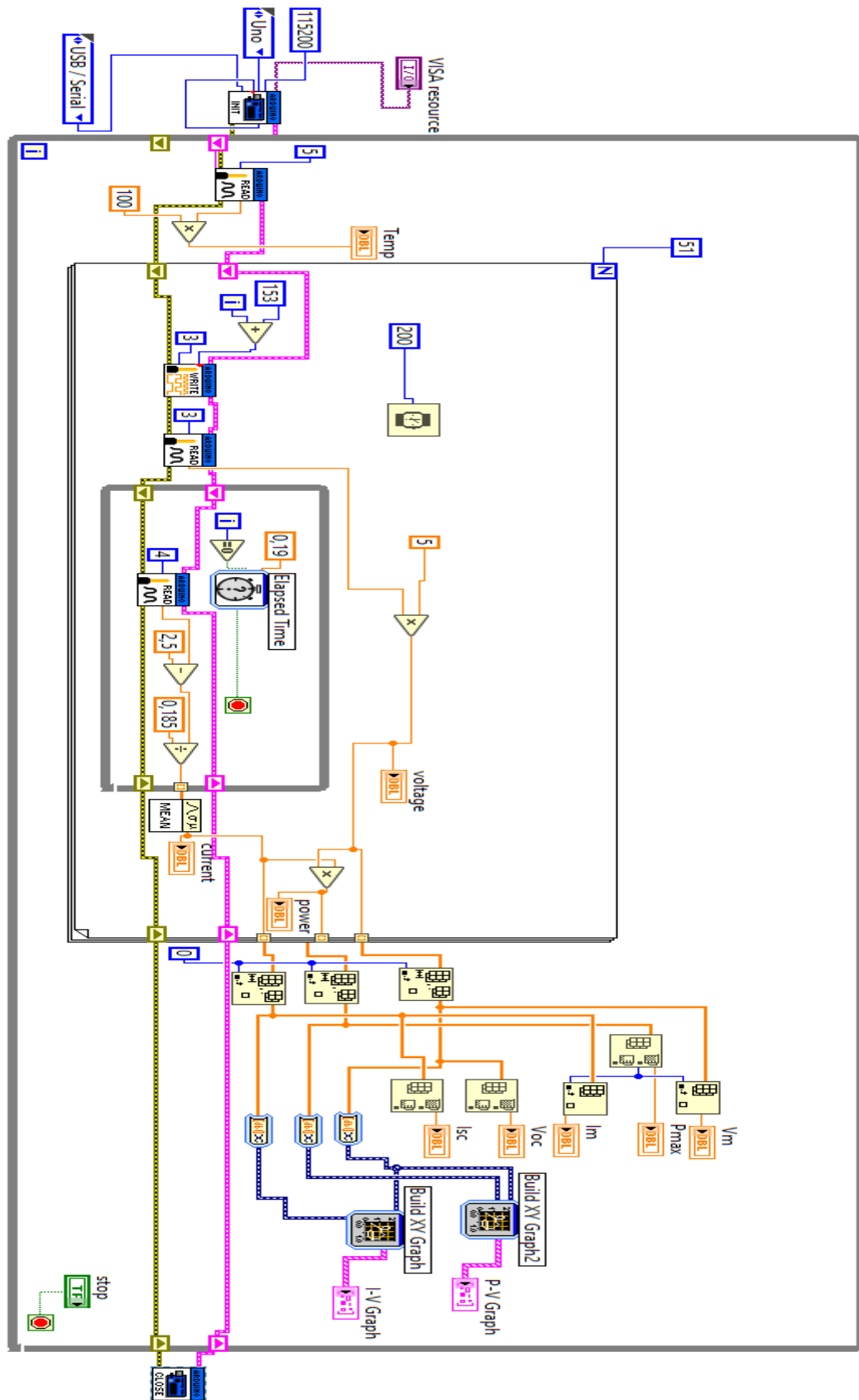


Figure 4.2 The Block Diagram.

Figure 4.2 represent the block diagram of this project, the program is divided into three parts:

- PWM signal generator

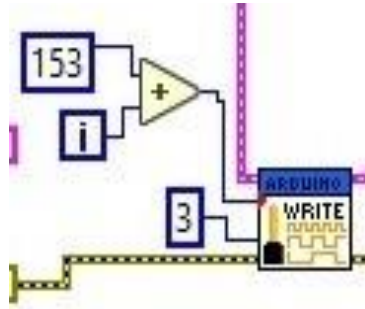


Figure 4.3 PWM Write Pin.

A PWM write pin is used for generating PWM signal, and for this task to take a place the Arduino pin is selected to be pin 3. The second step is to specify the duty cycle that must be between 60% and 80% which means that the specification of the PWM write pin must be between 153 and 204. It is done by using the variation of the iteration of the for loop by adding 153 to the first iteration to get the lower limit, and using the number of iteration to get the upper limit which is in this case 51 iteration.

- Read data

Three data sets have to be analysed (current, voltage and temperature), these data can be obtained using analogue read pin. First, the temperature data set is read through Arduino pin A5 using the following equation:

$$T = 100 * V_{in5} \quad (4.1)$$

Where T is the PV panel temperature and V_{in5} is the temperature sensor output.

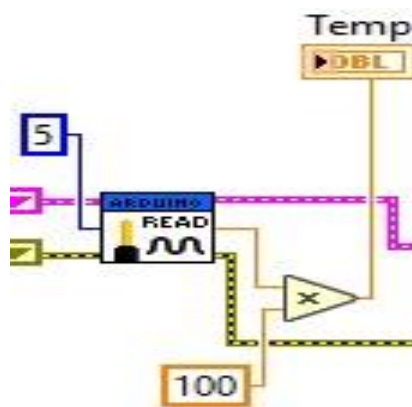


Figure 4.4 LabView Temp Measurement Block.

Furthermore, the voltage data set read through Arduino pin A3 based on the equation (4.2).

$$V = 5 * V_{in3} \quad (4.2)$$

Where V is the PV panel voltage and Vin3 is the voltage sensor output.

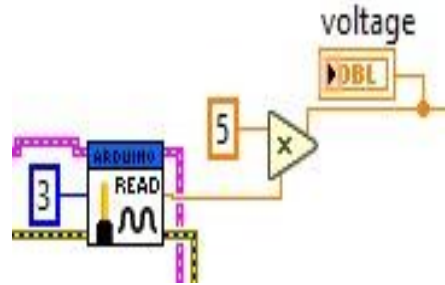


Figure 4.5 LabView Voltage Measurement Bloc.

Finally, the current data set goes through Arduino pin A4 using the following equation:

$$I = \frac{V_{in4} - 2.5}{0.185} \quad (4.3)$$

Where I is the PV panel current and Vin4 is current sensor output.

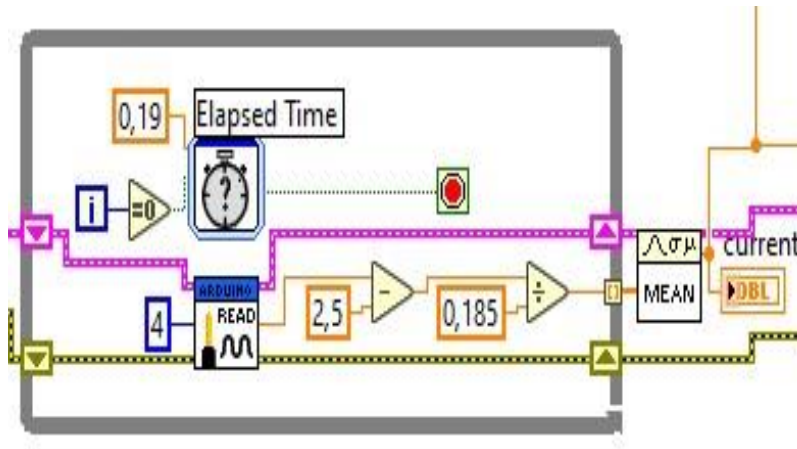


Figure 4.6 LabView Current Measurement Block.

Multiple measurements of PV current are averaged using a *while loop* and *elapsed time* to reduce current sensor errors.

- Calculation and display

All the values of current, voltage and power that measured before in the for loop should be indexed in arrays and then, the I-V and P-V graphs can be plotted by using " build XY graph" After that the other parameters such as I_{sh} , V_{OC} and P_{max} can be calculated by taking the maximum value of the current, voltage and power arrays respectively through the use of

Array Max & Min and display it. Calculate V_m and I_m using "display from array" by taking the index of P_{max} and display from voltage and current arrays respectively.

ii) Front Panel

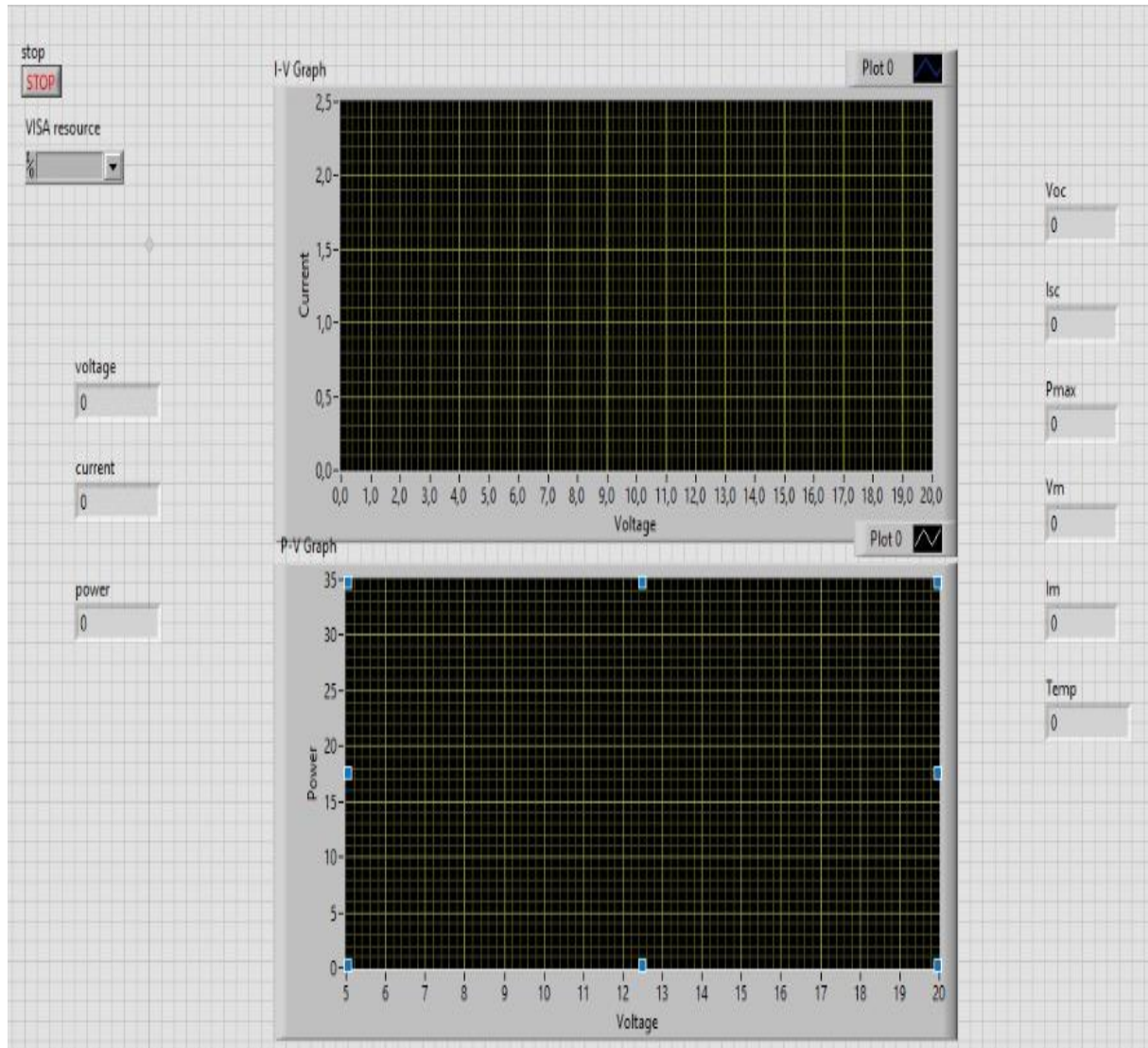
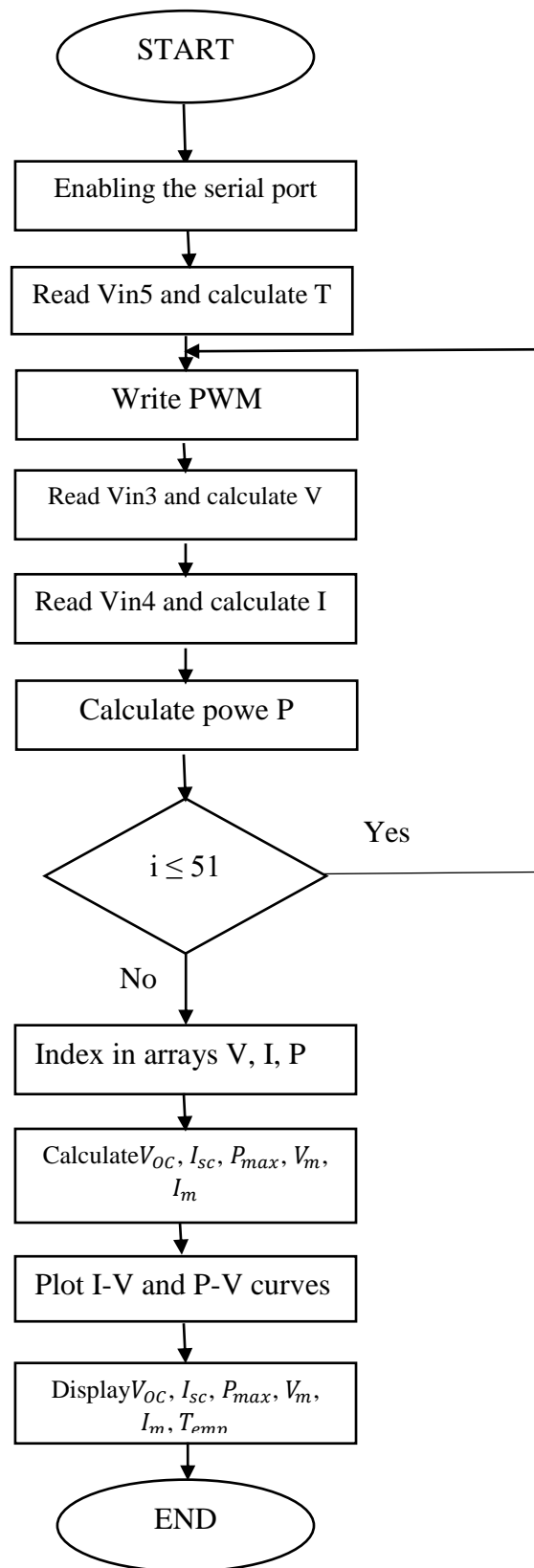


Figure 4.7 The Front Panel

Figure 4.3 shows the front panel of the LabVIEW program. It contains the IV and PV curves. It displays also the parameters of the PV panel which are: V_{OC} , I_{sc} , P_{max} , V_m , I_m , and T_{emp} .

iii) Flow Chart



4.3.2 Hardware Part

i) Schematic Diagram

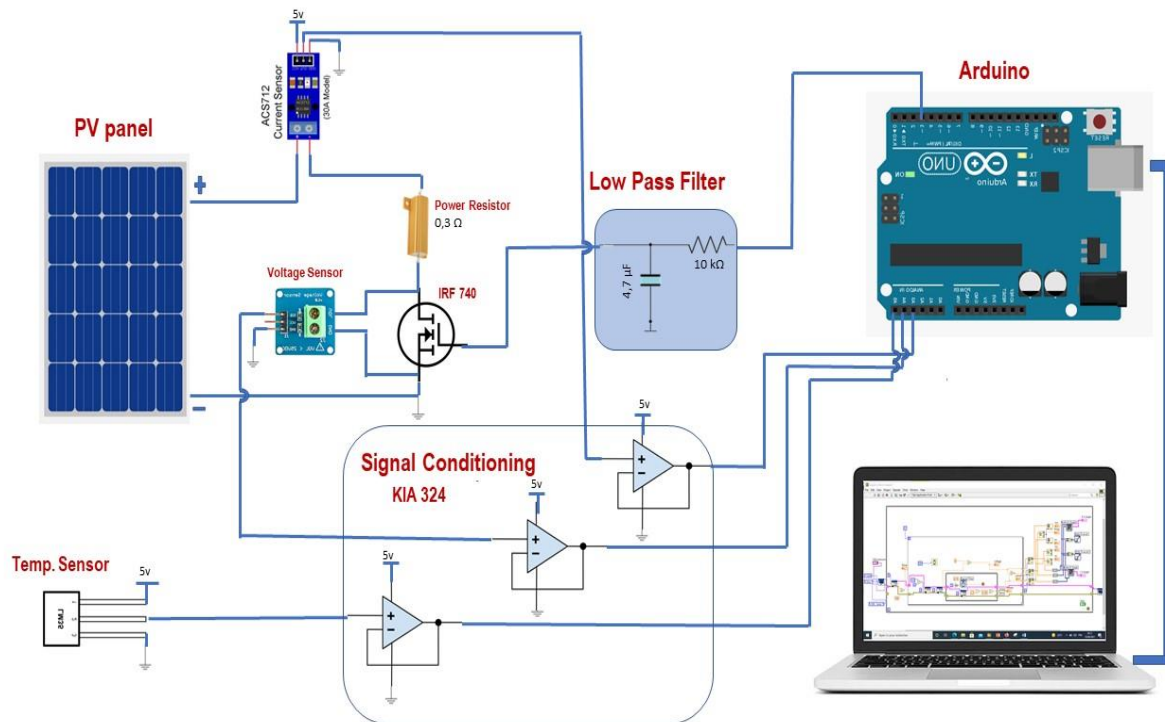


Figure 4.8 Schematic diagram.

ii) Components

As described in chapter3, the components used in this project are:

- PV panel (STP050D-12/MEA)
- Arduino
- Voltage Sensor
- Current Sensor (ACS712)
- Temperature Sensor (LM35)
- Signal Conditioning Circuit
- Power Resistance (0.2Ω)
- MOSFET IRF740: It is used to control the PV panel current and voltage which has a threshold and saturation voltage of 3 and 4 respectively. The MOSFET had a threshold voltage of 3V, this value allows the current to go through from source to the drain and reaches a maximum value at saturation voltage which is 4V.

- RC Filter: Resistor and Capacitor used to build up a first order low-pass filter. This low pass-filter is made with a resistor of $10K\Omega$ and capacitor of $4.7\mu F$ that results a time constant of 47ms which is greater than the PWM period (2ms), to ensure that the capacitor will never charge up and always taking the average value according to the duty cycle. As this latter changes from 60% to 82%, the analog voltage ranging from 3V to 4V.

4.3.3 Principle of Operation

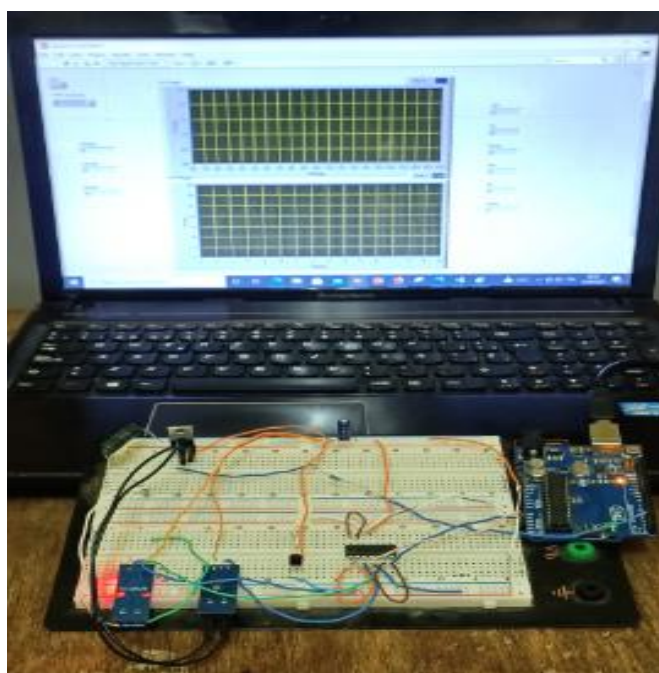


Figure 4.9 Circuit Implementation.

The PWM signal generated by the Arduino with a duty cycle variation between 60% and 82% is taken as the input for the low pass filter. This latter converts the signal to an analog voltage in a range of 3V- 4V. The output of the low pass filter is connected to the gate of the MOSFET, as the gate voltage increases the drain current also increases. A power resistor is connected between the positive terminal of the PV panel and the drain, the negative terminal of the PV panel is connected to the source of the MOSFET. When the gate voltage increases from 3V to 4V, the PV current increases from 0 to its maximum value (I_{sc}) dissimilar to the voltage that decreases from V_{oc} to its minimum value. The voltage sensor is connected in parallel with the drain and source of the MOSFET, and the current sensor is connected in series with the power resistor. These two sensors provide current and voltage data to Arduino through its pins 3 and 4 respectively, by using these data I-V and P-V curves can be plotted and the other parameters can be calculated.

4.4 Test Results and Discussion

4.4.1 First Test

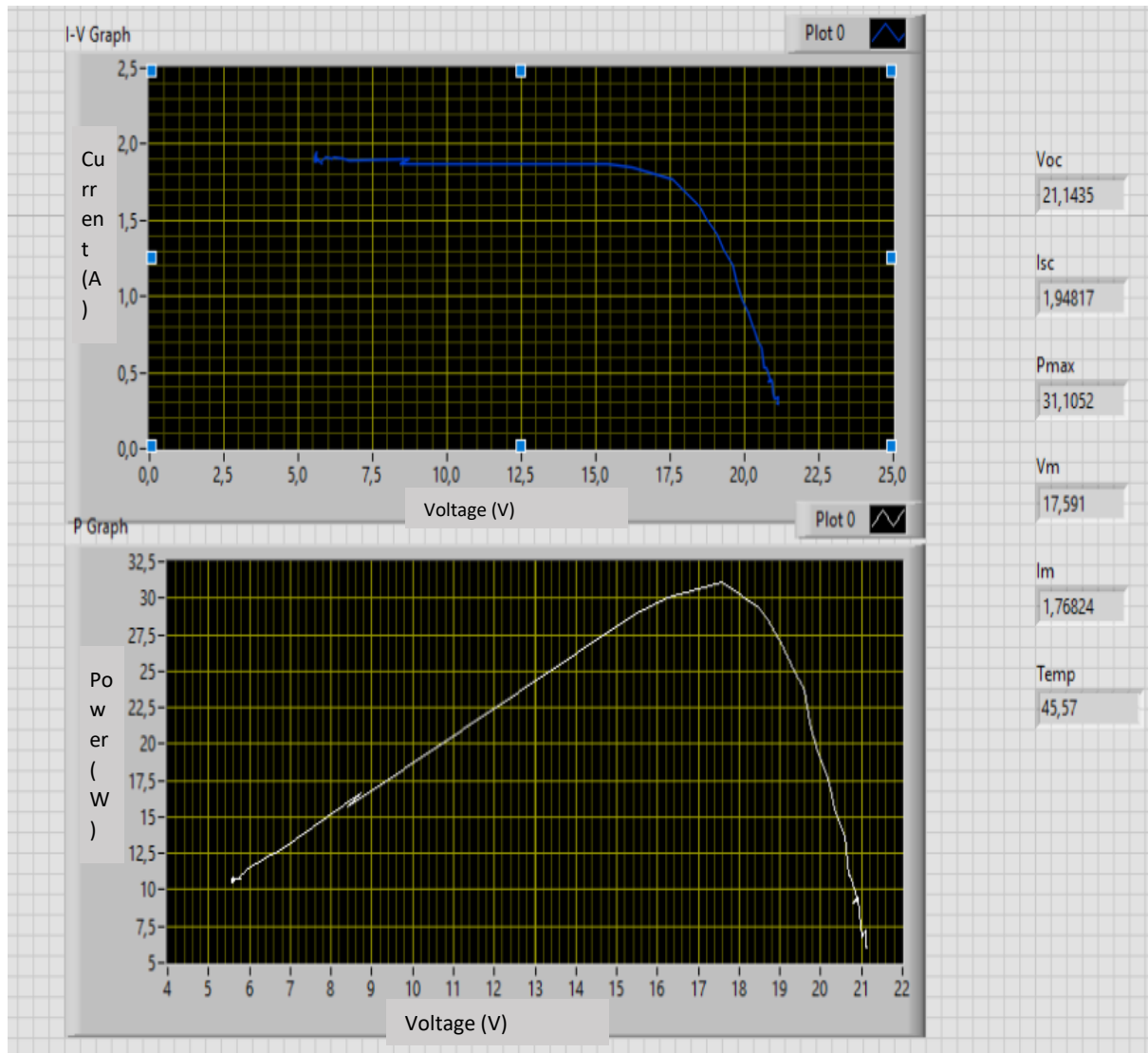


Figure 4.10 Test under conditions Temp. 45.57° and G 700 W/m².

This test was done under conditions with a temperature degree of 45.57° and an average irradiance (700 W/m²). The obtained results show that the parameters of this test are satisfied as shown in the real-time parameters display. In figure 4.10, it can be noticed that $V_{OC} = 21.14V$ and it is close to the value of 21.8V which is the manufacture's value V_{OC} . However, the test current which is 1.9A that is different from that of the short circuit current 3.13A mentioned in the data sheet given in appendix A that is due to the existing the internal resistance of the MOSFET in series with a power resistance of 0.3 Ω connected to the MOSFET, which means that the tested current is not a solid short-circuit without power resistance. The maximum power of 31 W can occur at voltage of 17.6 V.

For validation of the developed platform, experimental Data of the STP050D-12/MEA module that has been obtained in this test may be compared with the simulation results using the GWO based ODM Simulator developed in our research laboratory [22]. This demonstration and the accuracy can be seen in Figures 4.11.

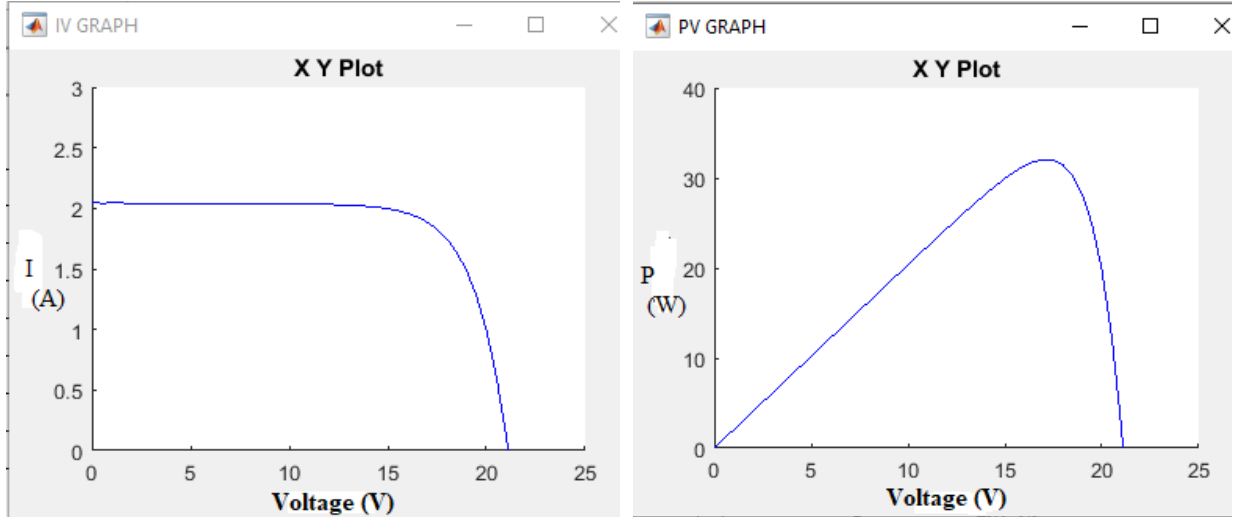


Figure 4.11 Simulation I-V and P-V characteristics

It can be noticed that the measured data obtained in our laboratory have small divergence compared to the simulation. Because, the irradiance value during the experiment is not well known due to the lack of irradiance sensor. Thus, the obtained I-V and P-V characteristics for the STP050D-12/MEA module based only on the datasheet information using the IOB-PSO simulation gives little bit good results due to the mentioned problem.

Thus, the results obtained by comparing the experimental and the simulation values are given in Table 4.1 with quit high relative error in I_{mpp} due the previous mentioned problem.

Table 2 Comparison of Experimental and simulation model values

Parameters	Experimental	Parameters from the simulation	Relative error (%)
	Parameters	of the model	
V_{mpp} [V]	17.6	17	3.53
I_{mpp} [A]	1.77	1.89	6.35
P_{max} [W]	31	32	3.25

4.4.2 Second Test (high temperature and high irradiance)

The second test is carried out under condition with high temperature and high irradiance as shown in Figure 4.12. A temperature of 50.96° which is higher than the first test, this resulted in a decrease of V_{OC} from 21.14V to 19.6V, because the open circuit voltage is the most affected parameter by the temperature. It can be noted that the current increases slightly to 2.25A, that's not only due to the increase of the temperature, but also due to the higher irradiance (sunny day). The maximum power of 34.2 W can occur at voltage of 15.5 V.

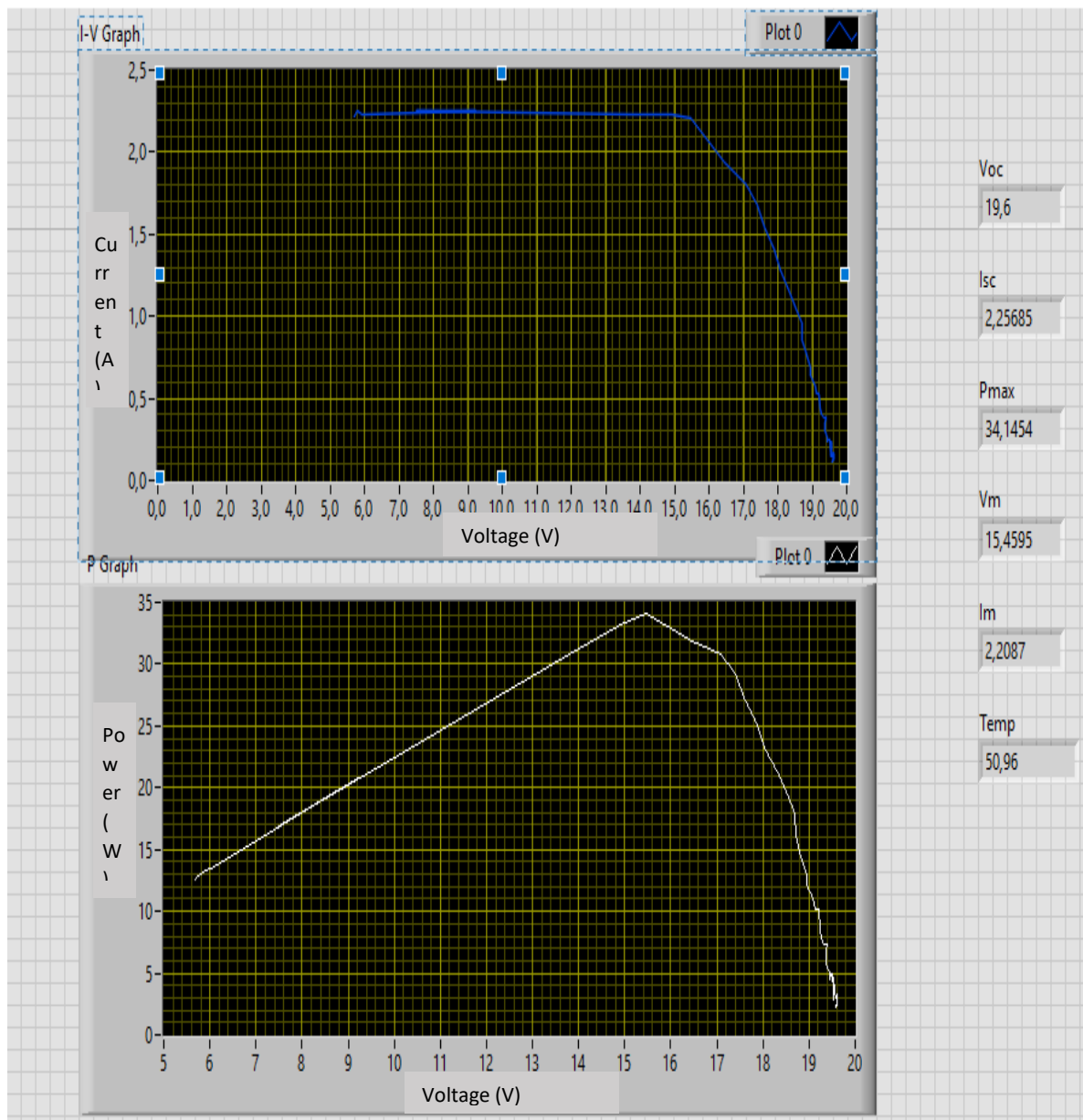


Figure 4.12 High temperature test (sunny day).

4.4.3 Effect of irradiance

The last test was carried out in a cloudy day which means the irradiance was very low, the PV panel short circuit current that is the most affected parameter, decreased significantly to 0.62A. Due to this weather condition, there was also a decrease in temperature yielding in a slight increase in the open circuit voltage to 23.39V. The maximum power of 12.5 W can occur at voltage of 20.3 V.

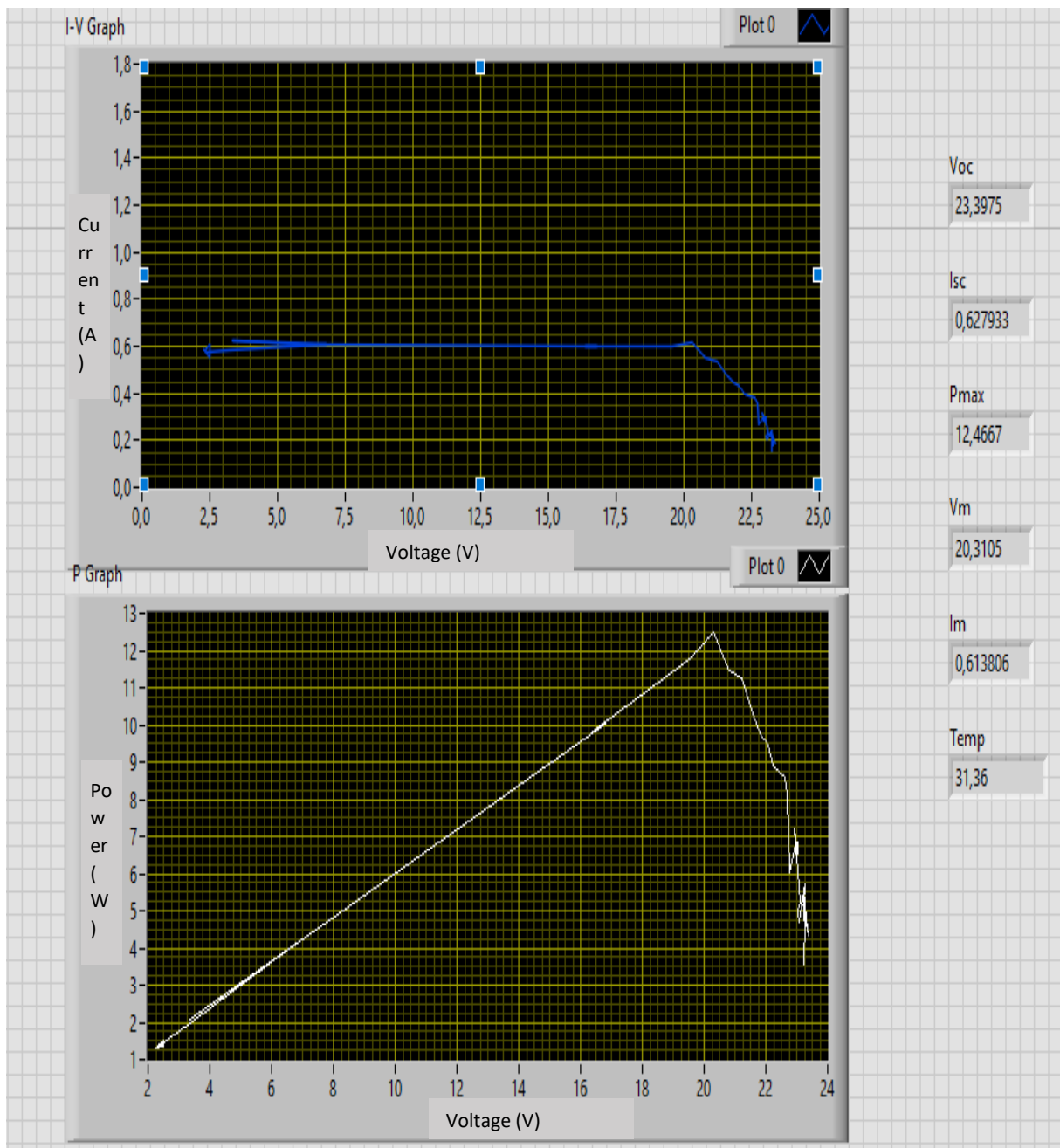


Figure 4.13 Low irradiance test (cloudy day).

4.5 Conclusion

This chapter presents the implementation of the project, besides the principles of operation of software and hardware parts in details. Moreover, three tests have been carried out under different conditions. The first test was performed under weather condition (Temp.45.57°, Average Irradiance), and the obtained results show data that are similar to expected value. In the second test, the maximum power that is higher than the first test can be obtained at a voltage lower than fist test, because both the temperature and irradiance are high. However, in the last test, the maximum power that can be obtained is the smallest one compared to the first and second test, besides, a maximum voltage can be obtained. These obtained data in the last test due to the weather condition, because both the temperature and irradiance are high.

All tests show how voltage and current can be affected by a change in irradiance and temperature.

Chapter 5

General Conclusion

General Conclusion

This report has presented the implementation of the new platform frame work using Labview, Ardouino and MOSFET for characterizing PV panel by plotting and saving the current-voltage I-V and P-V curves automatically.

This may open a door for further research to achieve the unachievable; a solar energy for producing electricity will be significantly developed.

The principles of operation of software and hardware parts have been also presented in details. For testing and validating this project, three tests have been carried out under different conditions. The first test was performed under weather condition (Temp.45.57°, Average Irradiance), and the obtained results show a good agreement with the expected ones. In the second test, the maximum power that is higher than the first test has been obtained at a voltage with the value lower than fist test, because both the temperature and irradiance are high. However in the last test, the maximum power that has been obtained is the smallest one compared to the first and second test, besides, a maximum voltage can be obtained. These obtained data in the last test are low due to the weather condition, because both the temperature and irradiance are low.

All tests show how voltage and current can be affected by a change in irradiance and temperature.

Furthermore, this project can be considered as a simple low cost system that can provide the I-V and P-V characteristics of any PV panels by using LabVIEW, Arduino, and simple MOSFET.

Moreover, the aforementioned system can be used for extracting any needed parameters under various environmental conditions. The combination of LabVIEW software program and open source Arduino Uno in leads to develop a program that is used for acquiring, displaying and saving the measured data on one hand. On the other hand, this developed program is used to control MOSFET using PWM technique.

Finally, this project has gone through many difficulties in its way to see light. The favorable obtained results during the tests are the hard evidence of the success of the

developed system. Thus, the system can help to characterize and analyze any PV panels and give the opportunity to fully enhance their generated power.

Bibliography

- [1] M. Kumar." Economic, and Environmental Impacts of Renewable Energy Resources". Wind Solar Hybrid Renewable Energy System,pp.1-2,2020.
- [2]J. Kumari, C. S. Babu. "Mathematical modeling and simulation of photovoltaic cell using matlab-simulink environment". International Journal of Electrical and Computer Engineering,vol.2,no.1,pp-26, 2012.
- [3]R. Faranda,S. Leva ." Energy comparison of MPPT techniques for PV Systems". WSEAS transactions on power systems,vol.3,no.6,pp. 446-455,2008.
- [4]R. Patel. "Design and Implementation of an Isolated Solar Photovoltaic Power Generation System", Doctoral dissertation,pp-7-8, 2014.
- [5] "Photovoltaic effect." Photovoltaic effect - Energy Education. [Online] Available: https://energyeducation.ca/encyclopedia/Photovoltaic_effect [Accessed : August 26, 2015].
- [6] B. Sudimac, A. Ugrinović, and M. Jurčević. " The application of photovoltaic systems in sacred buildings for the purpose of electric power production: The case study of the Cathedral of St. Michael the Archangel in Belgrade". Sustainability,vol.12,no.4,pp-1408,2020.
- [7] M.G. Villalva, J.R. Gazoli, and E. R. Filho. " Comprehensive approach to modeling and simulation of photovoltaic arrays". *IEEE Transactions on power electronics*,vol.24,no.5,pp-1198-1208,2009.
- [8] Y.Sawle,V.Tamrakar, and S. C .Gupta . " SINGLE-DIODE PV CELL MODELING AND STUDY OF CHARACTERISTICS OF SINGLE AND TOW-DIODE EQUIVALENT CIRCUIT".Electrical & Eletronics Engineering: An International Journal (ELEIJ),vol. 4,no.3,pp. 13-24,2015.
- [9] M.Cáceres, A.Firman, J.Montes-Romero, A. R. G.Mayans, L.H. Vera, E.F. Fernández, and J.de la Casa Higuera. "Low-Cost I–V Tracer for PV Modules under Real Operating Conditions".*Energies*,vol.13, no. 17,pp.4320.2020.
- [10] F. K. Rationelle Energiewandlung, Photovoltaic Systems Technology, 2003.
- [11] R.Chenni, M. Makhlof, T. Kerbache, and A. Bouzid. "A detailed modeling method for photovoltaic cells". *Energy*,vol. 32, no. 9,pp. 1724-1730,2007.

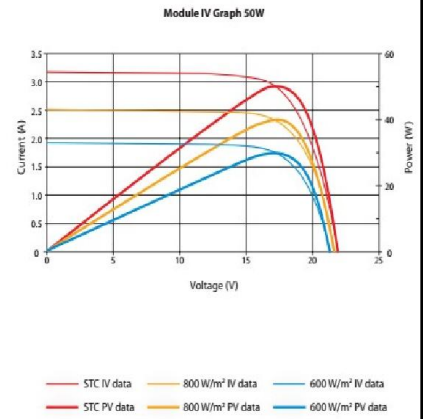
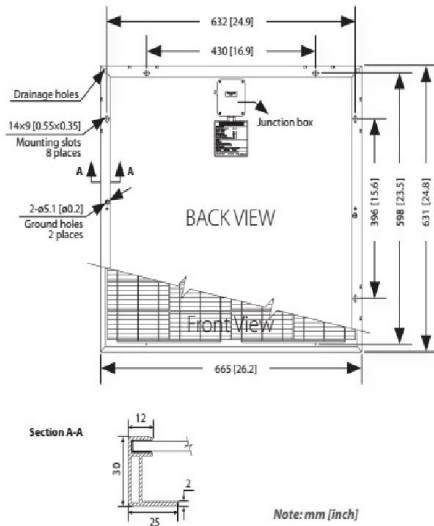
- [12] Significant Role of LabVIEW Database in SPC Software [Online].Available at: <https://intrastage.com/tag/labview-database/>[Accessed : August. 17,2021].
- [13] R. Bitter, T. Mohiuddin, and M. Nawrocki.” LabVIEW™ Advanced Programming Techniques: Advanced Programming Techniques”. CRC press,pp.1-37,2017.
- [14] R.H. Bishop.” Learning with labview”.PP.24-28,2015.
- [15] M. Schwartz, O. Manickum.” Programming Arduino with LabVIEW”. Packt Publishing Ltd,pp.5-9,2015.
- [16] STP050D-12/MEA [online] Available at: http://www.tehnosat.ro/pdf/PVmodules/Suntech_STP030D-12LEA_STP050D-12MEA.pdf [Accessed: August. 10, 2021].
- [17] *Arduino Uno Rev3* [online] Available at : <https://store.arduino.cc/arduino-uno-rev3/> [Accessed: August. 09,2021].
- [18] *MOSFET Characteristics* [Online].Available at: <https://www.electrical4u.com/mosfet-characteristics/>[Accessed: October. 28,2020].
- [19] *IRF Power MOSFET* [Online].Available at: <https://www.vishay.com/docs/91054/91054.pdf> [Accessed: August. 05, 2021].
- [20] *LM35 Data sheet* [Online]. Available at: <https://www.ti.com/lit/ds/symlink/lm35.pdf> [Accessed: August. 11, 2021].
- [21] *ACS712 Current Sensor Module* [Online]. Available at: <https://components101.com/sensors/acs712-current-sensor-module> [Accessed: August. 10,2021].
- [22] T.Cilina . "Photovoltaic cell I-V and P-V characteristics simulation versus measurement". Master Thesis, 2021.

Appendix-A

Data Sheet of PV Panel (STP050D-12/MEA)

SPECIFICATION CATEGORIES		Db Mono	Kb Poly	Cb Mono	Lb Poly	Rb Poly	Rb Poly	Md Poly	Md Poly	Sb Poly	Sb Poly	Sb Poly	Bb Mono	Bb Mono	Tb Poly	Tb Poly	Tb Poly
		STP005B -12/DEA	STP010D -12/KEA	STP020B -12/CEA	STP030D -12/LEA	STP040D -12/REA	STP045D -12/REA	STP050D -12/MEA	STP055D -12/MEA	STP060D -12/SEA	STP065D -12/SEA	STP070D -12/SEA	STP080B -12/BEA	STP085B -12/BEA	STP130D -12/TEA	STP135D -12/TEA	STP140D -12/TEA
ELECTRICAL CHARACTERISTICS	Open-Circuit Voltage (Voc)	21.6V	21.6V	21.7V	21.6V	21.8V	22.0V	21.8V	22.2V	21.6V	21.8V	22.0V	21.9V	22.2V	22.0V	22.3V	22.4V
	Optimum Operating Voltage (Vmp)	17.4V	17.4V	17.6V	17.2V	17.4V	17.6V	17.4V	17.5V	17.4V	17.6V	17.8V	17.5V	17.8V	17.4V	17.5V	17.6V
	Short-Circuit Current (Isc)	0.32A	0.65A	1.26A	1.94A	2.58A	2.79A	3.13A	3.34A	3.90A	4.11A	4.27A	4.95A	5.15A	8.09A	8.20A	8.33A
	Optimum Operating Current (Imp)	0.29A	0.57A	1.14A	1.74A	2.30A	2.58A	2.93A	3.14A	3.45A	3.69A	3.93A	4.58A	4.80A	7.47A	7.71A	7.95A
	Maximum Power at STC (Pmax)	5Wp	10Wp	20Wp	30Wp	40Wp	45Wp	50Wp	55Wp	60Wp	65Wp	70Wp	80Wp	85Wp	130Wp	135Wp	140Wp
	Operating Temperature	-40°C to +85°C	-40°C to +85°C	-40°C to +85°C	-40°C to +85°C	-40°C to +85°C	-40°C to +85°C	-40°C to +85°C	-40°C to +85°C	-40°C to +85°C	-40°C to +85°C	-40°C to +85°C	-40°C to +85°C	-40°C to +85°C	-40°C to +85°C	-40°C to +85°C	-40°C to +85°C
	Maximum System Voltage	715VDC	715VDC	715VDC	715VDC	715VDC	715VDC	715VDC	715VDC	715VDC	715VDC	715VDC	715VDC	715VDC	1000VDC	1000VDC	1000VDC
	Maximum Series Fuse Rating	5A	5A	5A	5A	10A	10A	10A	10A	15A	15A	15A	15A	15A	20A	20A	20A
	Power Tolerance	±10%	±10%	±10%	±10%	±5%	±5%	±5%	±5%	±5%	±5%	±5%	±5%	±5%	±5%	±5%	±5%
MECHANICAL CHARACTERISTICS	Solar Cell	Mono-crystalline solar cell	Poly-crystalline solar cell	Mono-crystalline solar cell	Poly-crystalline solar cell	Poly-crystalline solar cell	Poly-crystalline solar cell	Poly-crystalline solar cell	Poly-crystalline solar cell	Poly-crystalline solar cell	Poly-crystalline solar cell	Poly-crystalline solar cell	Mono-crystalline solar cell	Mono-crystalline solar cell	Poly-crystalline solar cell	Poly-crystalline solar cell	Poly-crystalline solar cell
	No. of Cells	36 (4x9)	36 (6x6)	36 (2x18)	36 (4x9)	36 (4x9)	36 (4x9)	36 (4x9)	36 (4x9)	36 (4x9)	36 (4x9)	36 (4x9)	36 (4x9)	36 (4x9)	36 (4x9)	36 (4x9)	36 (4x9)
	Dimensions	216 x 306 x 18 mm	310 x 368 x 18 mm	656 x 306 x 18 mm	426 x 680 x 18 mm	537 x 665 x 30 mm	537 x 665 x 30 mm	631 x 665 x 30 mm	631 x 665 x 30 mm	771 x 665 x 30 mm	771 x 665 x 30 mm	771 x 665 x 30 mm	1195 x 541 x 30 mm	1195 x 541 x 30 mm	1482 x 676 x 35 mm	1482 x 676 x 35 mm	1482 x 676 x 35 mm
	Weight	0.8 kgs	1.5 kgs	2.5 kgs	3.2 kgs	4.5 kgs	4.5 kgs	6.4 kgs	6.4 kgs	6.2 kgs	6.2 kgs	6.2 kgs	8.0 kgs	8.0 kgs	12.0 kgs	12.0 kgs	12.0 kgs
	Junction Box	IP65 rated	IP65 rated	IP65 rated	IP65 rated	IP65 rated	IP65 rated	IP65 rated	IP65 rated	IP65 rated	IP65 rated	IP65 rated	IP65 rated	IP65 rated	IP65 rated	IP65 rated	IP65 rated
	Output Cables	(Optional cable available)	(Optional cable available)	(Optional cable available)	(Optional cable available)	(Optional cable available)	(Optional cable available)	(Optional cable available)	(Optional cable available)	H+S (12 AWG) Lengths: 750mm(-) and 750mm(+) Connection: MC Plug Type IV	H+S (12 AWG) Lengths: 750mm(-) and 750mm(+) Connection: MC Plug Type IV	H+S (12 AWG) Lengths: 750mm(-) and 750mm(+) Connection: MC Plug Type IV	H+S (12 AWG) Lengths: 750mm(-) and 750mm(+) Connection: MC Plug Type IV	H+S (12 AWG) Lengths: 750mm(-) and 750mm(+) Connection: MC Plug Type IV	H+S (12 AWG) Lengths: 750mm(-) and 750mm(+) Connection: MC Plug Type IV	H+S (12 AWG) Lengths: 750mm(-) and 750mm(+) Connection: MC Plug Type IV	H+S (12 AWG) Lengths: 750mm(-) and 750mm(+) Connection: MC Plug Type IV
TEMP. CHARACTERISTICS	Nominal Operating Cell Temperature (NOCT)	45±2°C	45±2°C	45±2°C	45±2°C	45±2°C	45±2°C	45±2°C	45±2°C	45±2°C	45±2°C	45±2°C	45±2°C	45±2°C	45±2°C	45±2°C	45±2°C
	Temp. coefficient of Pmax	-0.48 %/°C	-0.47 %/°C	-0.48 %/°C	-0.47 %/°C	-0.48 %/°C	-0.48 %/°C	-0.47 %/°C	-0.47 %/°C	-0.47 %/°C	-0.47 %/°C	-0.47 %/°C	-0.48 %/°C	-0.48 %/°C	-0.47 %/°C	-0.47 %/°C	-0.47 %/°C
	Temp. coefficient of Voc	-0.34 %/°C	-0.34 %/°C	-0.34 %/°C	-0.34 %/°C	-0.34 %/°C	-0.34 %/°C	-0.34 %/°C	-0.34 %/°C	-0.34 %/°C	-0.34 %/°C	-0.34 %/°C	-0.34 %/°C	-0.34 %/°C	-0.34 %/°C	-0.34 %/°C	-0.34 %/°C
	Temp. coefficient of Isc	0.037 %/°C	0.045 %/°C	0.037 %/°C	0.045 %/°C	0.037 %/°C	0.037 %/°C	0.045 %/°C	0.045 %/°C	0.045 %/°C	0.045 %/°C	0.045 %/°C	0.037 %/°C	0.037 %/°C	0.045 %/°C	0.045 %/°C	0.045 %/°C

Md Poly STP050D-12/MEA

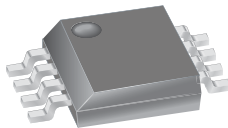


Fully Integrated, Hall Effect-Based Linear Current Sensor with 2.1 kVRMS Voltage Isolation and a Low-Resistance Current Conductor

Features and Benefits

- Low-noise analog signal path
- Device bandwidth is set via the new FILTER pin
- 5 μ s output rise time in response to step input current
- 50 kHz bandwidth
- Total output error 1.5% at $T_A = 25^\circ\text{C}$, and 4% at -40°C to 85°C
- Small footprint, low-profile SOIC8 package
- 1.2 m Ω internal conductor resistance
- 2.1 kV_{RMS} minimum isolation voltage from pins 1-4 to pins 5-8
- 5.0 V, single supply operation
- 66 to 185 mV/A output sensitivity
- Output voltage proportional to AC or DC currents
- Factory-trimmed for accuracy
- Extremely stable output offset voltage
- Nearly zero magnetic hysteresis
- Ratiometric output from supply voltage

Package: 8 pin SOIC (suffix LC)



Approximate Scale 1:1



Description

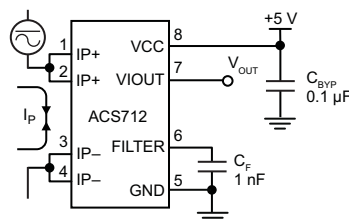
The Allegro[®] ACS712 provides economical and precise solutions for AC or DC current sensing in industrial, automotive, commercial, and communications systems. The device package allows for easy implementation by the customer. Typical applications include motor control, load detection and management, switched-mode power supplies, and overcurrent fault protection.

The device consists of a precise, low-offset, linear Hall sensor circuit with a copper conduction path located near the surface of the die. Applied current flowing through this copper conduction path generates a magnetic field which is sensed by the integrated Hall IC and converted into a proportional voltage. Device accuracy is optimized through the close proximity of the magnetic signal to the Hall transducer. A precise, proportional voltage is provided by the low-offset, chopper-stabilized BiCMOS Hall IC, which is programmed for accuracy after packaging.

The output of the device has a positive slope ($>V_{IOUT(Q)}$) when an increasing current flows through the primary copper conduction path (from pins 1 and 2, to pins 3 and 4), which is the path used for current sensing. The internal resistance of this conductive path is 1.2 m Ω typical, providing low power

Continued on the next page...

Typical Application



Application 1. The ACS712 outputs an analog signal, V_{OUT} , that varies linearly with the uni- or bi-directional AC or DC primary sensed current, I_P , within the range specified. C_F is recommended for noise management, with values that depend on the application.

ACS712

Fully Integrated, Hall Effect-Based Linear Current Sensor with 2.1 kVRMS Voltage Isolation and a Low-Resistance Current Conductor

Description (continued)

loss. The thickness of the copper conductor allows survival of the device at up to 5× overcurrent conditions. The terminals of the conductive path are electrically isolated from the sensor leads (pins 5 through 8). This allows the ACS712 current sensor to be used in applications requiring electrical isolation without the use of opto-isolators or other costly isolation techniques.

The ACS712 is provided in a small, surface mount SOIC8 package. The leadframe is plated with 100% matte tin, which is compatible with standard lead (Pb) free printed circuit board assembly processes. Internally, the device is Pb-free, except for flip-chip high-temperature Pb-based solder balls, currently exempt from RoHS. The device is fully calibrated prior to shipment from the factory.

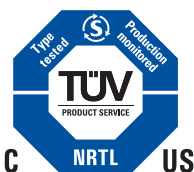
Selection Guide

Part Number	Packing*	T _{OP} (°C)	Optimized Range, I _P (A)	Sensitivity, Sens (Typ) (mV/A)
ACS712ELCTR-05B-T	Tape and reel, 3000 pieces/reel	–40 to 85	±5	185
ACS712ELCTR-20A-T	Tape and reel, 3000 pieces/reel	–40 to 85	±20	100
ACS712ELCTR-30A-T	Tape and reel, 3000 pieces/reel	–40 to 85	±30	66

*Contact Allegro for additional packing options.

Absolute Maximum Ratings

Characteristic	Symbol	Notes	Rating	Units
Supply Voltage	V _{CC}		8	V
Reverse Supply Voltage	V _{RCC}		–0.1	V
Output Voltage	V _{IOUT}		8	V
Reverse Output Voltage	V _{RIOUT}		–0.1	V
Output Current Source	I _{IOUT(SOURCE)}		3	mA
Output Current Sink	I _{IOUT(SINK)}		10	mA
Overcurrent Transient Tolerance	I _P	100 total pulses, 250 ms duration each, applied at a rate of 1 pulse every 100 seconds.	60	A
Maximum Transient Sensed Current	I _{R(max)}	Junction Temperature, T _J < T _{J(max)}	60	A
Nominal Operating Ambient Temperature	T _A	Range E	–40 to 85	°C
Maximum Junction	T _{J(max)}		165	°C
Storage Temperature	T _{stg}		–65 to 170	°C



TÜV America
Certificate Number:
U8V 06 05 54214 010

Parameter	Specification
Fire and Electric Shock	CAN/CSA-C22.2 No. 60950-1-03 UL 60950-1:2003 EN 60950-1:2001

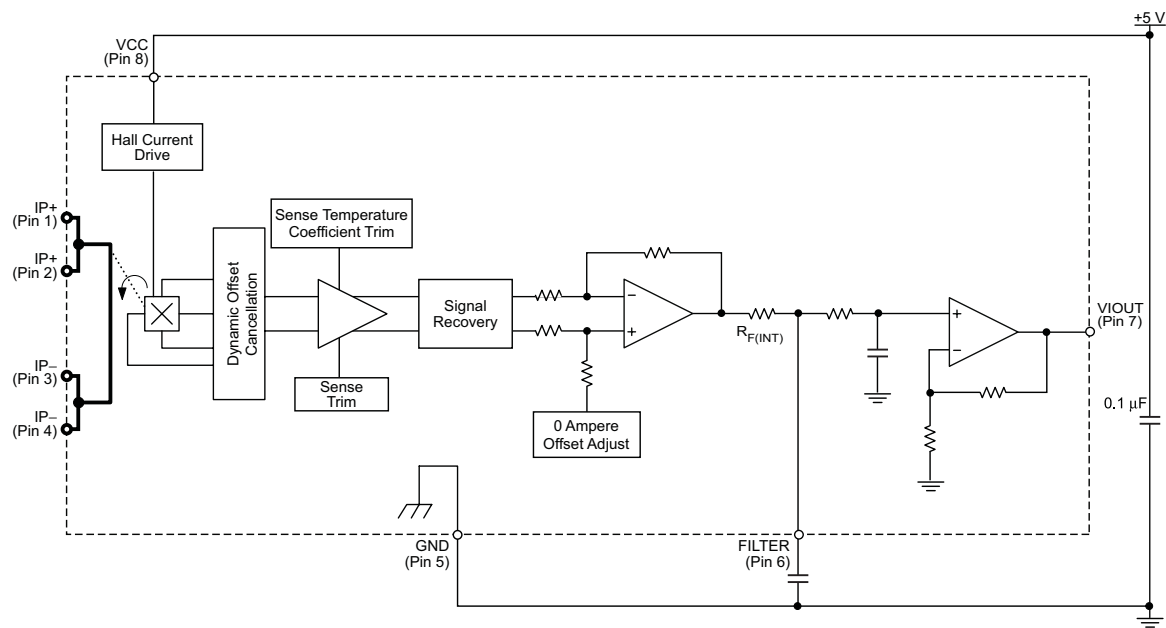


Allegro MicroSystems, Inc.
115 Northeast Cutoff, Box 15036
Worcester, Massachusetts 01615-0036 (508) 853-5000
www.allegromicro.com

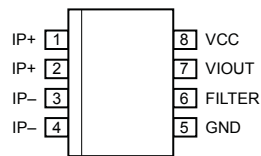
ACS712

Fully Integrated, Hall Effect-Based Linear Current Sensor with
2.1 kVRMS Voltage Isolation and a Low-Resistance Current Conductor

Functional Block Diagram



Pin-out Diagram



Terminal List Table

Number	Name	Description
1 and 2	IP+	Terminals for current being sensed; fused internally
3 and 4	IP-	Terminals for current being sensed; fused internally
5	GND	Signal ground terminal
6	FILTER	Terminal for external capacitor that sets bandwidth
7	VIOUT	Analog output signal
8	VCC	Device power supply terminal

COMMON OPERATING CHARACTERISTICS¹ over full range of T_{OP} , $C_F = 1$ nF, and $V_{CC} = 5$ V, unless otherwise specified

Characteristic	Symbol	Test Conditions	Min.	Typ.	Max.	Units
ELECTRICAL CHARACTERISTICS						
Supply Voltage	V_{CC}		4.5	5.0	5.5	V
Supply Current	I_{CC}	$V_{CC} = 5.0$ V, output open	6	8	11	mA
Output Zener Clamp Voltage	V_Z	$I_{CC} = 11$ mA, $T_A = 25^\circ\text{C}$	6	8.3	—	V
Output Resistance	R_{IOUT}	$I_{IOUT} = 1.2$ mA, $T_A = 25^\circ\text{C}$	—	1	2	Ω
Output Capacitance Load	C_{LOAD}	V _{IOUT} to GND	—	—	10	nF
Output Resistive Load	R_{LOAD}	V _{IOUT} to GND	4.7	—	—	k Ω
Primary Conductor Resistance	$R_{PRIMARY}$	$T_A = 25^\circ\text{C}$	—	1.2	—	m Ω
RMS Isolation Voltage	V_{ISORMS}	Pins 1-4 and 5-8; 60 Hz, 1 minute, $T_A = 25^\circ\text{C}$	2100	—	—	V
DC Isolation Voltage	V_{ISODC}	Pins 1-4 and 5-8; 1 minute, $T_A = 25^\circ\text{C}$	—	5000	—	V
Propagation Time	t_{PROP}	$I_P = I_P(\text{max})$, $T_A = 25^\circ\text{C}$, $C_{OUT} = \text{open}$	—	3	—	μs
Response Time	$t_{RESPONSE}$	$I_P = I_P(\text{max})$, $T_A = 25^\circ\text{C}$, $C_{OUT} = \text{open}$	—	7	—	μs
Rise Time	t_r	$I_P = I_P(\text{max})$, $T_A = 25^\circ\text{C}$, $C_{OUT} = \text{open}$	—	5	—	μs
Frequency Bandwidth	f	−3 dB, $T_A = 25^\circ\text{C}$; I_P is 10 A peak-to-peak	50	—	—	kHz
Nonlinearity	E_{LIN}	Over full range of I_P	—	±1	±1.5	%
Symmetry	E_{SYM}	Over full range of I_P	98	100	102	%
Zero Current Output Voltage	$V_{IOUT(Q)}$	Bidirectional; $I_P = 0$ A, $T_A = 25^\circ\text{C}$	—	$V_{CC} \times 0.5$	—	V
Magnetic Offset Error	V_{ERROM}	$I_P = 0$ A, after excursion of 5 A	—	0	—	mV
Clamping Voltage	V_{CH}		Typ. −110	$V_{CC} \times 0.9375$	Typ. +110	mV
	V_{CL}		Typ. −110	$V_{CC} \times 0.0625$	Typ. +110	mV
Power-On Time	t_{PO}	Output reaches 90% of steady-state level, $T_J = 25^\circ\text{C}$, 20 A present on leadframe	—	35	—	μs
Magnetic Coupling ²			—	12	—	G/A
Internal Filter Resistance ³	$R_{F(INT)}$			1.7		k Ω

¹Device may be operated at higher primary current levels, I_P , and ambient, T_A , and internal leadframe temperatures, T_{OP} , provided that the Maximum Junction Temperature, $T_J(\text{max})$, is not exceeded.

²1G = 0.1 mT.

³ $R_{F(INT)}$ forms an RC circuit via the FILTER pin.

COMMON THERMAL CHARACTERISTICS¹

			Min.	Typ.	Max.	Units
Operating Internal Leadframe Temperature	T_{OP}	E range	−40	—	85	$^\circ\text{C}$
Junction-to-Lead Thermal Resistance ²	$R_{\theta JL}$	Mounted on the Allegro ASEK 712 evaluation board			5	$^\circ\text{C/W}$
Junction-to-Ambient Thermal Resistance	$R_{\theta JA}$	Mounted on the Allegro 85-0322 evaluation board, includes the power consumed by the board			23	$^\circ\text{C/W}$

¹Additional thermal information is available on the Allegro website.

²The Allegro evaluation board has 1500 mm² of 2 oz. copper on each side, connected to pins 1 and 2, and to pins 3 and 4, with thermal vias connecting the layers. Performance values include the power consumed by the PCB. Further details on the board are available from the Frequently Asked Questions document on our website. Further information about board design and thermal performance also can be found in the Applications Information section of this datasheet.

ACS712

Fully Integrated, Hall Effect-Based Linear Current Sensor with 2.1 kVRMS Voltage Isolation and a Low-Resistance Current Conductor

x05A PERFORMANCE CHARACTERISTICS $T_{OP} = -40^{\circ}\text{C}$ to 85°C ¹, $C_F = 1\text{ nF}$, and $V_{CC} = 5\text{ V}$, unless otherwise specified

Characteristic	Symbol	Test Conditions	Min.	Typ.	Max.	Units
Optimized Accuracy Range	I_P		-5	—	5	A
Sensitivity ²	$Sens_{TA}$	Over full range of I_P , $T_A = 25^{\circ}\text{C}$	—	185	—	mV/A
	$Sens_{TOP}$	Over full range of I_P	178	—	193	mV/A
Noise	$V_{NOISE(PP)}$	Peak-to-peak, $T_A = 25^{\circ}\text{C}$, 185 mV/A programmed Sensitivity, $C_F = 4.7\text{ nF}$, $C_{OUT} = \text{open}$, 20 kHz bandwidth	—	45	—	mV
		Peak-to-peak, $T_A = 25^{\circ}\text{C}$, 185 mV/A programmed Sensitivity, $C_F = 47\text{ nF}$, $C_{OUT} = \text{open}$, 2 kHz bandwidth	—	20	—	mV
		Peak-to-peak, $T_A = 25^{\circ}\text{C}$, 185 mV/A programmed Sensitivity, $C_F = 1\text{ nF}$, $C_{OUT} = \text{open}$, 50 kHz bandwidth	—	75	—	mV
Electrical Offset Voltage	V_{OE}	$I_P = 0\text{ A}$	-40	—	40	mV
Total Output Error ³	E_{TOT}	$I_P = \pm 5\text{ A}$, $T_A = 25^{\circ}\text{C}$	—	± 1.5	—	%

¹Device may be operated at higher primary current levels, I_P , and ambient temperatures, T_{OP} , provided that the Maximum Junction Temperature, $T_{J(max)}$, is not exceeded.

²At -40°C Sensitivity may shift as much 9% outside of the datasheet limits.

³Percentage of I_P , with $I_P = 5\text{ A}$. Output filtered.

x20A PERFORMANCE CHARACTERISTICS $T_{OP} = -40^{\circ}\text{C}$ to 85°C ¹, $C_F = 1\text{ nF}$, and $V_{CC} = 5\text{ V}$, unless otherwise specified

Characteristic	Symbol	Test Conditions	Min.	Typ.	Max.	Units
Optimized Accuracy Range	I_P		-20	—	20	A
Sensitivity ²	$Sens_{TA}$	Over full range of I_P , $T_A = 25^{\circ}\text{C}$	—	100	—	mV/A
	$Sens_{TOP}$	Over full range of I_P	97	—	103	mV/A
Noise	$V_{NOISE(PP)}$	Peak-to-peak, $T_A = 25^{\circ}\text{C}$, 100 mV/A programmed Sensitivity, $C_F = 4.7\text{ nF}$, $C_{OUT} = \text{open}$, 20 kHz bandwidth	—	24	—	mV
		Peak-to-peak, $T_A = 25^{\circ}\text{C}$, 100 mV/A programmed Sensitivity, $C_F = 47\text{ nF}$, $C_{OUT} = \text{open}$, 2 kHz bandwidth	—	10	—	mV
		Peak-to-peak, $T_A = 25^{\circ}\text{C}$, 100 mV/A programmed Sensitivity, $C_F = 1\text{ nF}$, $C_{OUT} = \text{open}$, 50 kHz bandwidth	—	40	—	mV
Electrical Offset Voltage	V_{OE}	$I_P = 0\text{ A}$	-30	—	30	mV
Total Output Error ³	E_{TOT}	$I_P = \pm 20\text{ A}$, $T_A = 25^{\circ}\text{C}$	—	± 1.5	—	%

¹Device may be operated at higher primary current levels, I_P , and ambient temperatures, T_{OP} , provided that the Maximum Junction Temperature, $T_{J(max)}$, is not exceeded.

²At -40°C Sensitivity may shift as much 9% outside of the datasheet limits.

³Percentage of I_P , with $I_P = 20\text{ A}$. Output filtered.

x30A PERFORMANCE CHARACTERISTICS $T_{OP} = -40^{\circ}\text{C}$ to 85°C ¹, $C_F = 1\text{ nF}$, and $V_{CC} = 5\text{ V}$, unless otherwise specified

Characteristic	Symbol	Test Conditions	Min.	Typ.	Max.	Units
Optimized Accuracy Range	I_P		-30	—	30	A
Sensitivity ²	$Sens_{TA}$	Over full range of I_P , $T_A = 25^{\circ}\text{C}$	—	66	—	mV/A
	$Sens_{TOP}$	Over full range of I_P	64	—	68	mV/A
Noise	$V_{NOISE(PP)}$	Peak-to-peak, $T_A = 25^{\circ}\text{C}$, 66 mV/A programmed Sensitivity, $C_F = 4.7\text{ nF}$, $C_{OUT} = \text{open}$, 20 kHz bandwidth	—	20	—	mV
		Peak-to-peak, $T_A = 25^{\circ}\text{C}$, 66 mV/A programmed Sensitivity, $C_F = 47\text{ nF}$, $C_{OUT} = \text{open}$, 2 kHz bandwidth	—	7	—	mV
		Peak-to-peak, $T_A = 25^{\circ}\text{C}$, 66 mV/A programmed Sensitivity, $C_F = 1\text{ nF}$, $C_{OUT} = \text{open}$, 50 kHz bandwidth	—	35	—	mV
Electrical Offset Voltage	V_{OE}	$I_P = 0\text{ A}$	-30	—	30	mV
Total Output Error ³	E_{TOT}	$I_P = \pm 30\text{ A}$, $T_A = 25^{\circ}\text{C}$	—	± 1.5	—	%

¹Device may be operated at higher primary current levels, I_P , and ambient temperatures, T_{OP} , provided that the Maximum Junction Temperature, $T_{J(max)}$, is not exceeded.

²At -40°C Sensitivity may shift as much 9% outside of the datasheet limits.

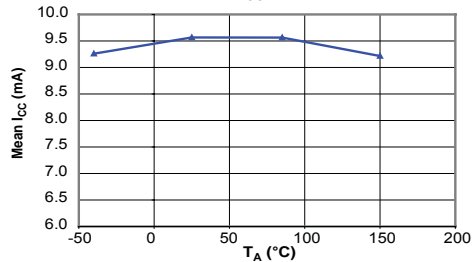
³Percentage of I_P , with $I_P = 30\text{ A}$. Output filtered.



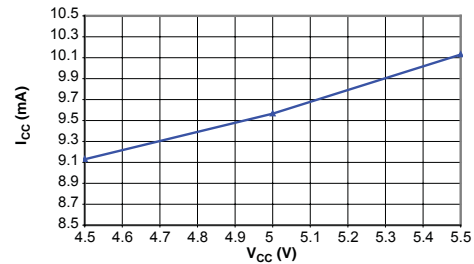
Characteristic Performance

$I_P = 5\text{ A}$, Sens = 185 mV/A unless otherwise specified

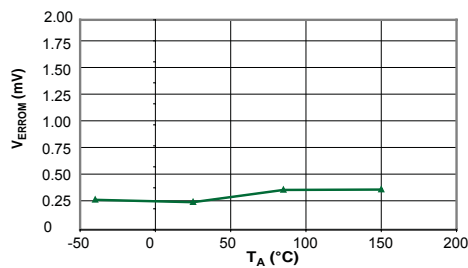
Mean Supply Current versus Ambient Temperature
 $V_{CC} = 5\text{ V}$



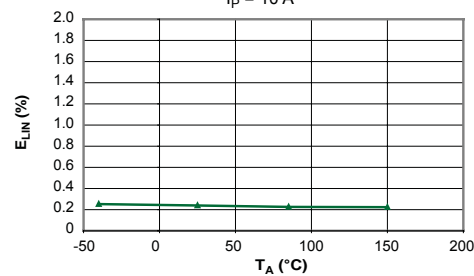
Supply Current versus Supply Voltage



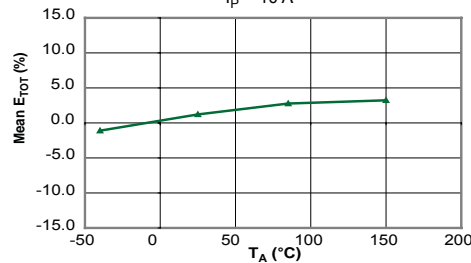
Magnetic Offset versus Ambient Temperature



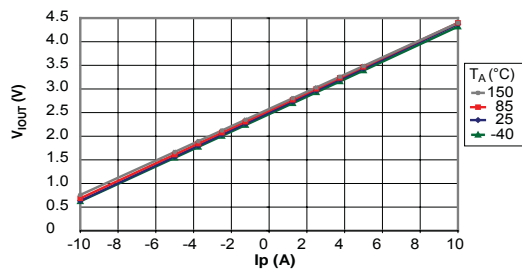
Nonlinearity versus Ambient Temperature
 $I_P = 10\text{ A}$



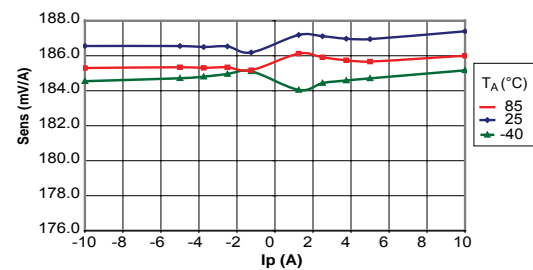
Mean Total Output Error versus Ambient Temperature
 $I_P = 10\text{ A}$



Output Voltage versus Sensed Current



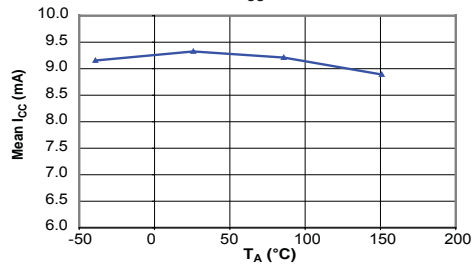
Sensitivity versus Sensed Current



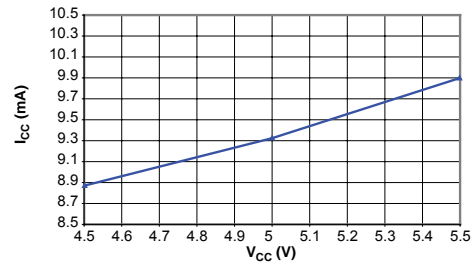
Characteristic Performance

$I_P = 30\text{ A}$, Sens = 66 mV/A unless otherwise specified

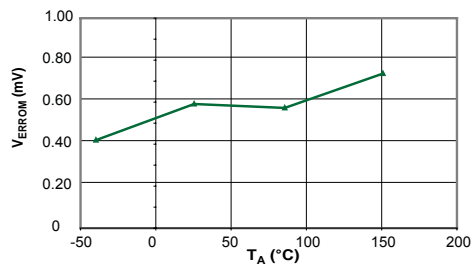
Mean Supply Current versus Ambient Temperature
 $V_{CC} = 5\text{ V}$



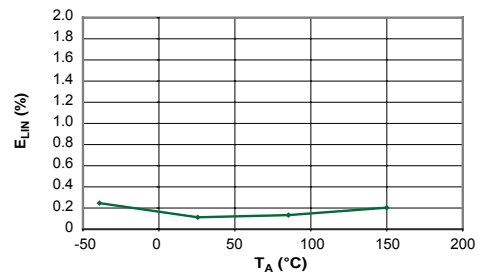
Supply Current versus Supply Voltage



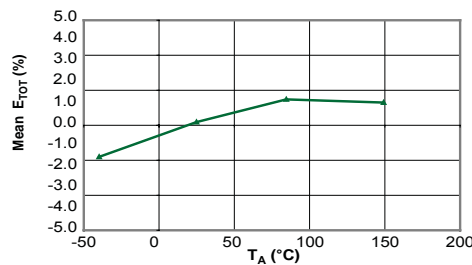
Magnetic Offset Current versus Ambient Temperature



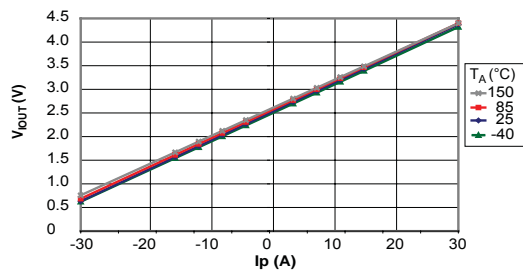
Nonlinearity versus Ambient Temperature



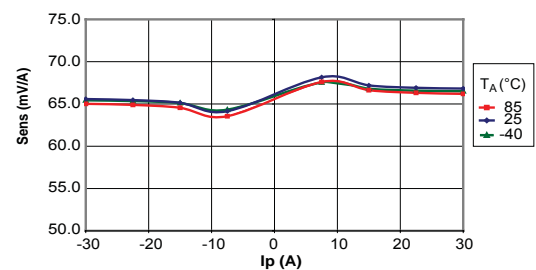
Mean Total Output Error versus Ambient Temperature



Output Voltage versus Sensed Current



Sensitivity versus Sensed Current



Definitions of Accuracy Characteristics

Sensitivity (Sens). The change in sensor output in response to a 1 A change through the primary conductor. The sensitivity is the product of the magnetic circuit sensitivity (G/A) and the linear IC amplifier gain (mV/G). The linear IC amplifier gain is programmed at the factory to optimize the sensitivity (mV/A) for the full-scale current of the device.

Noise (V_{NOISE}). The product of the linear IC amplifier gain (mV/G) and the noise floor for the Allegro Hall effect linear IC (≈ 1 G). The noise floor is derived from the thermal and shot noise observed in Hall elements. Dividing the noise (mV) by the sensitivity (mV/A) provides the smallest current that the device is able to resolve.

Linearity (E_{LIN}). The degree to which the voltage output from the sensor varies in direct proportion to the primary current through its full-scale amplitude. Nonlinearity in the output can be attributed to the saturation of the flux concentrator approaching the full-scale current. The following equation is used to derive the linearity:

$$100 \left\{ 1 - \left[\frac{\Delta \text{ gain} \times \% \text{ sat} (V_{\text{IOUT_full-scale amperes}} - V_{\text{IOUT(Q)}})}{2 (V_{\text{IOUT_half-scale amperes}} - V_{\text{IOUT(Q)}})} \right] \right\}$$

where $V_{\text{IOUT_full-scale amperes}}$ = the output voltage (V) when the sensed current approximates full-scale $\pm I_p$.

Symmetry (E_{SYM}). The degree to which the absolute voltage output from the sensor varies in proportion to either a positive or negative full-scale primary current. The following formula is used to derive symmetry:

$$100 \left(\frac{V_{\text{IOUT_+ full-scale amperes}} - V_{\text{IOUT(Q)}}}{V_{\text{IOUT(Q)}} - V_{\text{IOUT_full-scale amperes}}} \right)$$

Quiescent output voltage ($V_{\text{IOUT(Q)}}$). The output of the sensor when the primary current is zero. For a unipolar supply voltage, it nominally remains at $V_{\text{CC}}/2$. Thus, $V_{\text{CC}} = 5$ V translates into $V_{\text{IOUT(Q)}} = 2.5$ V. Variation in $V_{\text{IOUT(Q)}}$ can be attributed to the resolution of the Allegro linear IC quiescent voltage trim and thermal drift.

Electrical offset voltage (V_{OE}). The deviation of the device output from its ideal quiescent value of $V_{\text{CC}}/2$ due to nonmagnetic causes. To convert this voltage to amperes, divide by the device sensitivity, Sens.

Accuracy (E_{TOT}). The accuracy represents the maximum deviation of the actual output from its ideal value. This is also known as the total output error. The accuracy is illustrated graphically in the output voltage versus current chart at right.

Accuracy is divided into four areas:

- **0 A at 25°C.** Accuracy of sensing zero current flow at 25°C, without the effects of temperature.
- **0 A over Δ temperature.** Accuracy of sensing zero current flow including temperature effects.
- **Full-scale current at 25°C.** Accuracy of sensing the full-scale current at 25°C, without the effects of temperature.
- **Full-scale current over Δ temperature.** Accuracy of sensing full-scale current flow including temperature effects.

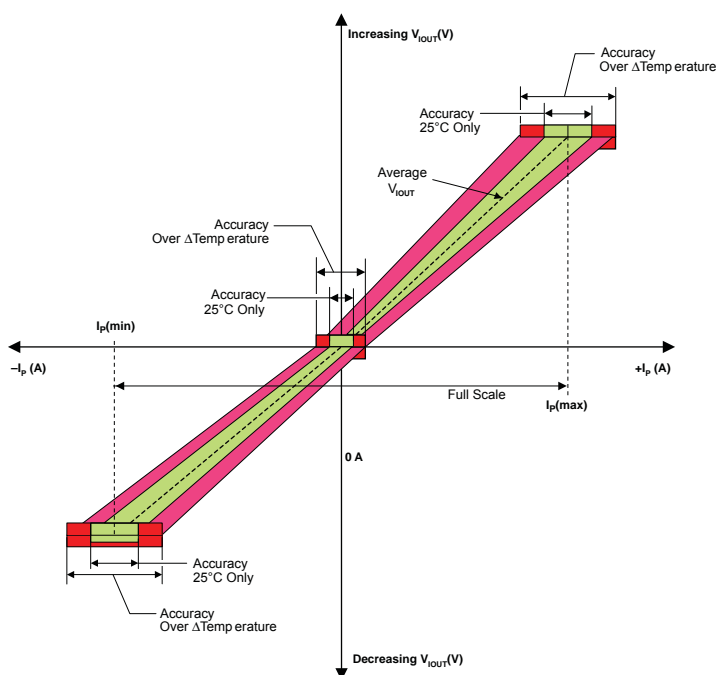
Ratiometry. The ratiometric feature means that its 0 A output, $V_{\text{IOUT(Q)}}$, (nominally equal to $V_{\text{CC}}/2$) and sensitivity, Sens, are proportional to its supply voltage, V_{CC} . The following formula is used to derive the ratiometric change in 0 A output voltage, $\Delta V_{\text{IOUT(Q)RAT}}$ (%).

$$100 \left(\frac{V_{\text{IOUT(Q)VCC}} / V_{\text{IOUT(Q)5V}}}{V_{\text{CC}} / 5 \text{ V}} \right)$$

The ratiometric change in sensitivity, $\Delta \text{Sens}_{\text{RAT}}$ (%), is defined as:

$$100 \left(\frac{\text{Sens}_{\text{VCC}} / \text{Sens}_{5\text{V}}}{V_{\text{CC}} / 5 \text{ V}} \right)$$

Output Voltage versus Sensed Current
Accuracy at 0 A and at Full-Scale Current

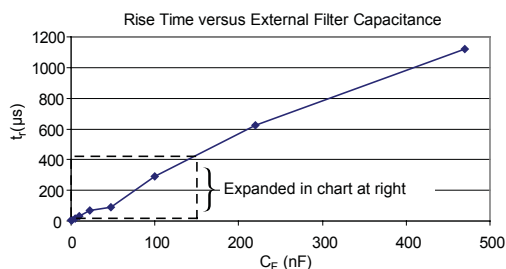
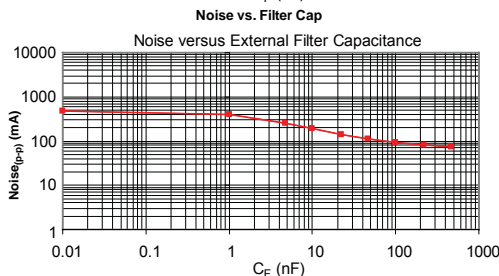
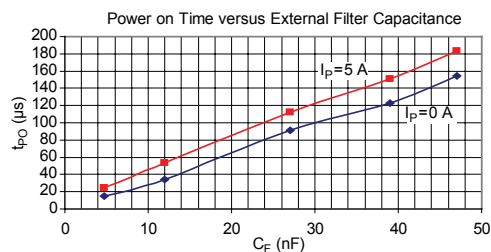
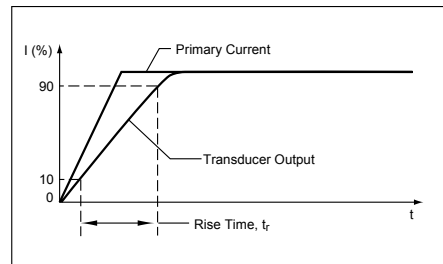
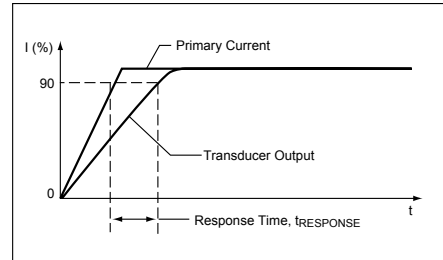
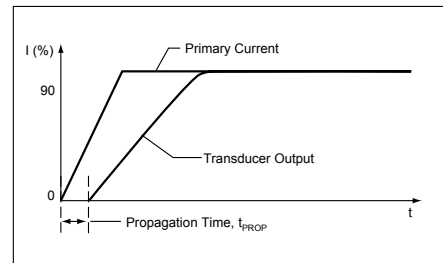


Definitions of Dynamic Response Characteristics

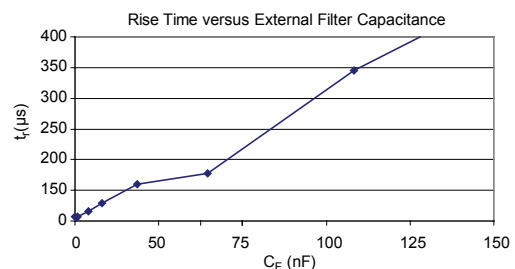
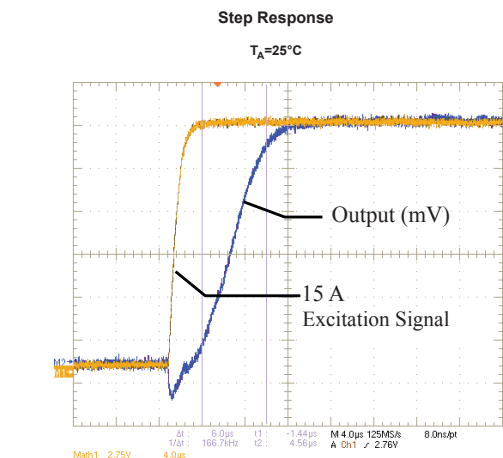
Propagation delay (t_{PROP}). The time required for the sensor output to reflect a change in the primary current signal. Propagation delay is attributed to inductive loading within the linear IC package, as well as in the inductive loop formed by the primary conductor geometry. Propagation delay can be considered as a fixed time offset and may be compensated.

Response time ($t_{RESPONSE}$). The time interval between a) when the primary current signal reaches 90% of its final value, and b) when the sensor reaches 90% of its output corresponding to the applied current.

Rise time (t_r). The time interval between a) when the sensor reaches 10% of its full scale value, and b) when it reaches 90% of its full scale value. The rise time to a step response is used to derive the bandwidth of the current sensor, in which $f(-3\text{ dB}) = 0.35/t_r$. Both t_r and $t_{RESPONSE}$ are detrimentally affected by eddy current losses observed in the conductive IC ground plane.



C_F (nF)	t_r (μs)
0	6.6
1	7.7
4.7	17.4
10	32.1
22	68.2
47	88.2
100	291.3
220	623.0
470	1120.0



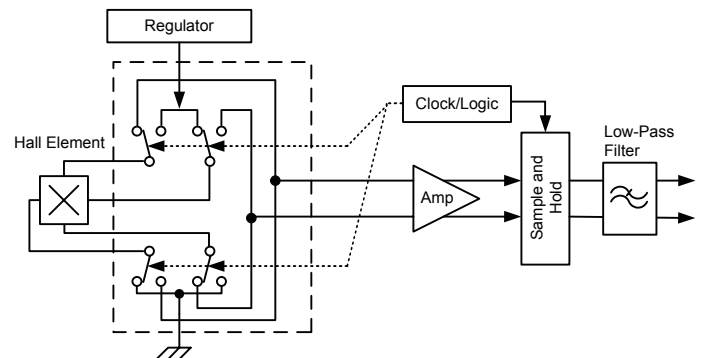
ACS712

Fully Integrated, Hall Effect-Based Linear Current Sensor with 2.1 kVRMS Voltage Isolation and a Low-Resistance Current Conductor

Chopper Stabilization Technique

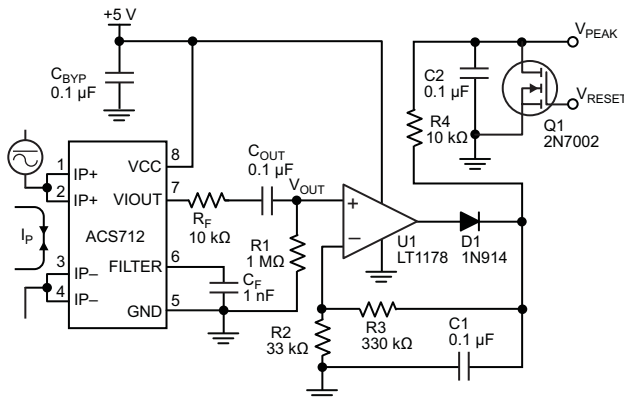
Chopper Stabilization is an innovative circuit technique that is used to minimize the offset voltage of a Hall element and an associated on-chip amplifier. Allegro patented a Chopper Stabilization technique that nearly eliminates Hall IC output drift induced by temperature or package stress effects. This offset reduction technique is based on a signal modulation-demodulation process. Modulation is used to separate the undesired dc offset signal from the magnetically induced signal in the frequency domain. Then, using a low-pass filter, the modulated dc offset is suppressed while the magnetically induced signal passes through the filter. As a result of this chopper stabilization approach, the output voltage from the Hall IC is desensitized to the effects of temperature and mechanical stress. This technique produces devices that have an extremely stable Electrical Offset Voltage, are immune to thermal stress, and have precise recoverability after temperature cycling.

This technique is made possible through the use of a BiCMOS process that allows the use of low-offset and low-noise amplifiers in combination with high-density logic integration and sample and hold circuits.

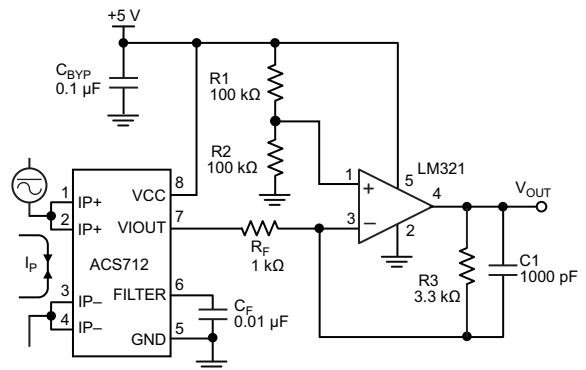


Concept of Chopper Stabilization Technique

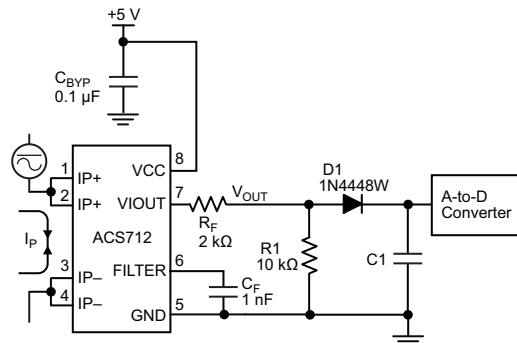
Typical Applications



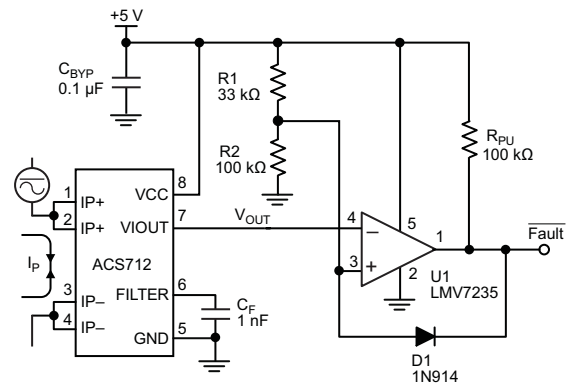
Application 2. Peak Detecting Circuit



Application 3. This configuration increases gain to 610 mV/A (tested using the ACS712ELC-05A).



Application 4. Rectified Output. 3.3 V scaling and rectification application for A-to-D converters. Replaces current transformer solutions with simpler ACS circuit. C1 is a function of the load resistance and filtering desired. R1 can be omitted if the full range is desired.



Application 5. 10 A Overcurrent Fault Latch. Fault threshold set by R1 and R2. This circuit latches an overcurrent fault and holds it until the 5 V rail is powered down.

Improving Sensing System Accuracy Using the FILTER Pin

In low-frequency sensing applications, it is often advantageous to add a simple RC filter to the output of the sensor. Such a low-pass filter improves the signal-to-noise ratio, and therefore the resolution, of the sensor output signal. However, the addition of an RC filter to the output of a sensor IC can result in undesirable sensor output attenuation — even for dc signals.

Signal attenuation, ΔV_{ATT} , is a result of the resistive divider effect between the resistance of the external filter, R_F (see Application 6), and the input impedance and resistance of the customer interface circuit, R_{INTFC} . The transfer function of this resistive divider is given by:

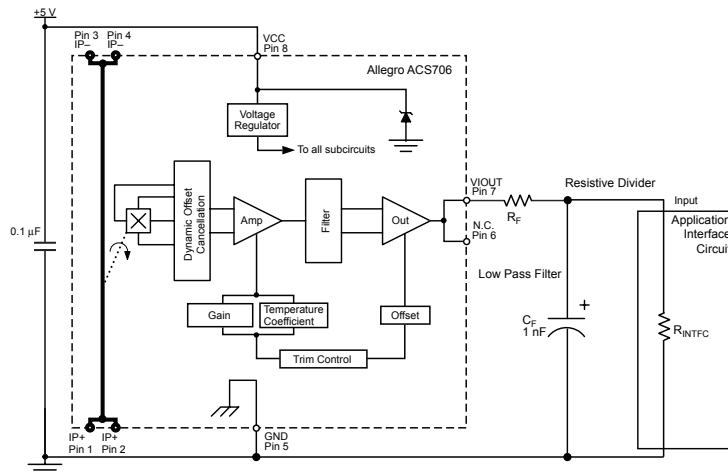
$$\Delta V_{ATT} = V_{IOUT} \left(\frac{R_{INTFC}}{R_F + R_{INTFC}} \right)$$

Even if R_F and R_{INTFC} are designed to match, the two individual resistance values will most likely drift by different amounts over

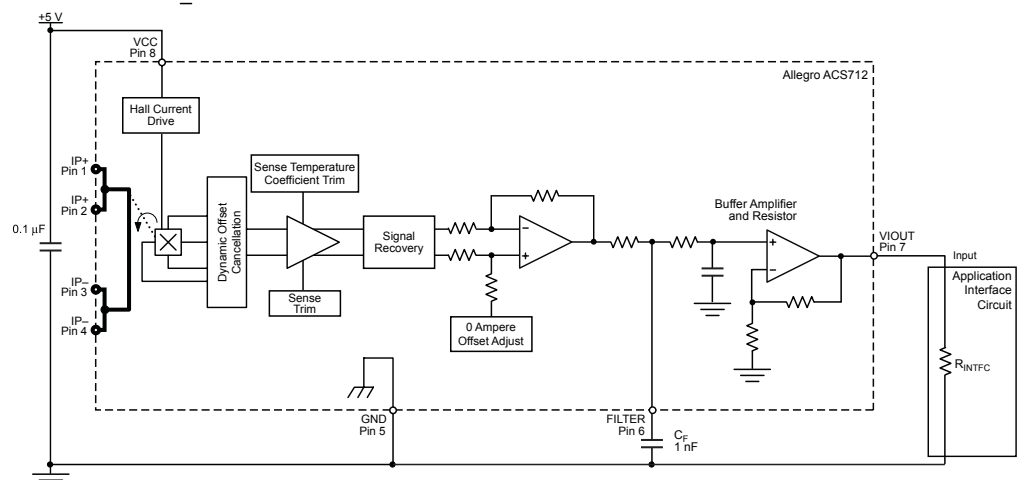
temperature. Therefore, signal attenuation will vary as a function of temperature. Note that, in many cases, the input impedance, R_{INTFC} , of a typical analog-to-digital converter (ADC) can be as low as 10 k Ω .

The ACS712 contains an internal resistor, a FILTER pin connection to the printed circuit board, and an internal buffer amplifier. With this circuit architecture, users can implement a simple RC filter via the addition of a capacitor, C_F (see Application 7) from the FILTER pin to ground. The buffer amplifier inside of the ACS712 (located after the internal resistor and FILTER pin connection) eliminates the attenuation caused by the resistive divider effect described in the equation for ΔV_{ATT} . Therefore, the ACS712 device is ideal for use in high-accuracy applications that cannot afford the signal attenuation associated with the use of an external RC low-pass filter.

Application 6. When a low pass filter is constructed externally to a standard Hall effect device, a resistive divider may exist between the filter resistor, R_F , and the resistance of the customer interface circuit, R_{INTFC} . This resistive divider will cause excessive attenuation, as given by the transfer function for ΔV_{ATT} .



Application 7. Using the FILTER pin provided on the ACS712 eliminates the attenuation effects of the resistor divider between R_F and R_{INTFC} , shown in Application 6.



Fully Integrated, Hall Effect-Based Linear Current Sensor with 2.1 kVRMS Voltage Isolation and a Low-Resistance Current Conductor

e LC, 8-pin SOIC

Preliminary dimensions, for reference only
Dimensions in millimeters
U.S. Customary dimensions (in.) in brackets, for reference only
(reference JEDEC MS-012 AA)
Dimensions exclusive of mold flash, gate burrs, and dambar protrusions
Exact case and lead configuration at supplier discretion within limits shown

△ Terminal #1 mark area

The drawing shows three views of the e LC, 8-pin SOIC package:

- Top View:** Shows the package body with a triangular mark area (△) on the left. Dimensions include a width of 6.20 mm (.244 in.) with a tolerance of ±0.228 mm, and a pin pitch of 0.25 mm (.010 in.) with a tolerance of ±0.010 mm. The total width of the pin array is 5.00 mm (.197 in.) with a tolerance of ±0.189 mm. The distance from the mark area to the center of the pin array is 4.80 mm (.189 in.). The distance from the center of the pin array to the right edge is 4.00 mm (.157 in.) with a tolerance of ±0.150 mm. The distance from the center of the pin array to the right edge of the package body is 3.80 mm (.150 in.).
- Side View:** Shows the package height and lead configuration. The total height is 1.27 mm (.050 in.) with a tolerance of ±0.016 in. The distance from the base to the top of the package body is 0.40 mm (.016 in.). The lead angle is 8°.
- End View:** Shows the pin configuration and seating plane. The distance from the seating plane to the top of the package body is 1.75 mm (.069 in.) with a tolerance of ±0.053 in. The distance from the seating plane to the bottom of the package body is 1.35 mm (.053 in.). The distance from the seating plane to the bottom of the lead is 0.25 mm (.010 in.) with a tolerance of ±0.004 in. The distance from the seating plane to the bottom of the lead is 0.10 mm (.004 in.).

1							8
2							7
3							6
4							5

Text 1
Text 2
Text 3

ACS712T RLCPPP YYWWA	ACS 712 T	Allegro Current Sensor Device family number Indicator of 100% matte tin leadframe plating
	R LC PPP	Operating ambient temperature range code Package type designator Primary sensed current
	YY	Date code: Calendar year (last two digits)
	WW A	Date code: Calendar week Date code: Shift code

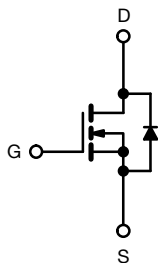
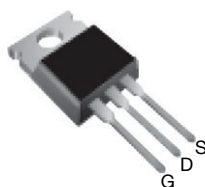
ACS712T <i>RLCPPP</i> <i>L...L</i> <i>YYWW</i>	ACS 712 T	Allegro Current Sensor Device family number Indicator of 100% matte tin leadframe plating
	<i>R</i> LC <i>PPP</i>	Operating ambient temperature range code Package type designator Primary sensed current
	<i>L...L</i>	Lot code
	<i>YY</i> <i>WW</i>	Date code: Calendar year (last two digits) Date code: Calendar week

Allegro MicroSystems, Inc. reserves the right to make, from time to time, such departures from the detail specifications as may be required to permit improvements in the performance, reliability,

Copyright ©2006, Allegro MicroSystems, Inc.



Power MOSFET

TO-220AB


N-Channel MOSFET

FEATURES

- Dynamic dV/dt rating
- Repetitive avalanche rated
- Fast switching
- Ease of paralleling
- Simple drive requirements
- Material categorization: for definitions of compliance please see www.vishay.com/doc?99912


RoHS*
Available

Note

* This datasheet provides information about parts that are RoHS-compliant and / or parts that are non RoHS-compliant. For example, parts with lead (Pb) terminations are not RoHS-compliant. Please see the information / tables in this datasheet for details

DESCRIPTION

Third generation power MOSFETs from Vishay provide the designer with the best combination of fast switching, ruggedized device design, low on-resistance and cost-effectiveness.

The TO-220AB package is universally preferred for all commercial-industrial applications at power dissipation levels to approximately 50 W. The low thermal resistance and low package cost of the TO-220AB contribute to its wide acceptance throughout the industry.

PRODUCT SUMMARY

V_{DS} (V)	400
$R_{DS(on)}$ (Ω)	$V_{GS} = 10\text{ V}$ 0.55
Q_g max. (nC)	63
Q_{gs} (nC)	9.0
Q_{gd} (nC)	32
Configuration	Single

ORDERING INFORMATION

Package	TO-220AB
Lead (Pb)-free	IRF740PbF
Lead (Pb)-free and halogen-free	IRF740PbF-BE3

ABSOLUTE MAXIMUM RATINGS ($T_C = 25\text{ }^\circ\text{C}$, unless otherwise noted)

PARAMETER	SYMBOL	LIMIT	UNIT
Drain-source voltage	V_{DS}	400	V
Gate-source voltage	V_{GS}	± 20	
Continuous drain current	I_D	10	A
		6.3	
Pulsed drain current ^a	I_{DM}	40	
Linear derating factor		1.0	W/ $^\circ\text{C}$
Single pulse avalanche energy ^b	E_{AS}	520	mJ
Repetitive avalanche current ^a	I_{AR}	10	A
Repetitive avalanche energy ^a	E_{AR}	13	mJ
Maximum power dissipation	P_D	125	W
Peak diode recovery dV/dt ^c	dV/dt	4.0	V/ns
Operating junction and storage temperature range	T_J, T_{stg}	-55 to +150	$^\circ\text{C}$
Soldering recommendations (peak temperature) ^d	For 10 s	300	
Mounting torque	6-32 or M3 screw	10	lbf · in
		1.1	N · m

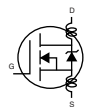
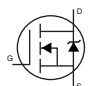
Notes

- Repetitive rating; pulse width limited by maximum junction temperature (see fig. 11)
- $V_{DD} = 50\text{ V}$, starting $T_J = 25\text{ }^\circ\text{C}$, $L = 9.1\text{ mH}$, $R_g = 25\text{ }\Omega$, $I_{AS} = 10\text{ A}$ (see fig. 12)
- $I_{SD} \leq 10\text{ A}$, $dI/dt \leq 120\text{ A}/\mu\text{s}$, $V_{DD} \leq V_{DS}$, $T_J \leq 150\text{ }^\circ\text{C}$
- 1.6 mm from case

**THERMAL RESISTANCE RATINGS**

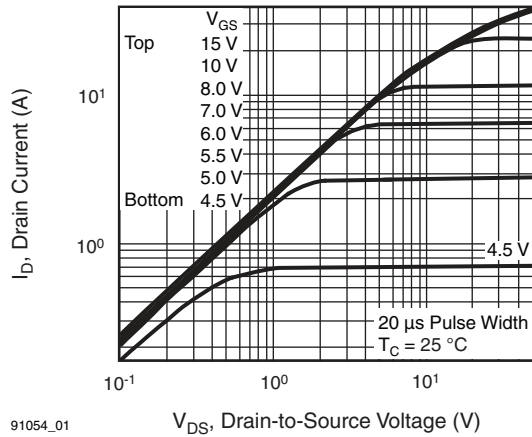
PARAMETER	SYMBOL	TYP.	MAX.	UNIT
Maximum junction-to-ambient	R_{thJA}	-	62	°C/W
Case-to-sink, flat, greased surface	R_{thCS}	0.50	-	
Maximum junction-to-case (drain)	R_{thJC}	-	1.0	

SPECIFICATIONS ($T_J = 25\text{ }^{\circ}\text{C}$, unless otherwise noted)

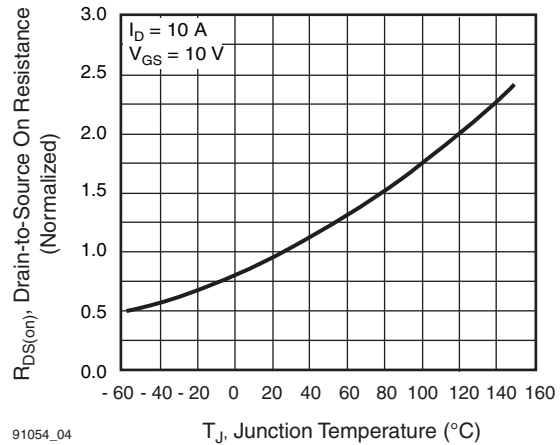
PARAMETER	SYMBOL	TEST CONDITIONS		MIN.	TYP.	MAX.	UNIT
Static							
Drain-source breakdown voltage	V_{DS}	$V_{GS} = 0\text{ V}$, $I_D = 250\text{ }\mu\text{A}$		400	-	-	V
V_{DS} temperature coefficient	$\Delta V_{DS}/T_J$	Reference to $25\text{ }^{\circ}\text{C}$, $I_D = 1\text{ mA}$		-	0.49	-	V/ $^{\circ}\text{C}$
Gate-source threshold voltage	$V_{GS(th)}$	$V_{DS} = V_{GS}$, $I_D = 250\text{ }\mu\text{A}$		2.0	-	4.0	V
Gate-source leakage	I_{GSS}	$V_{GS} = \pm 20\text{ V}$		-	-	± 100	nA
Zero gate voltage drain current	I_{DSS}	$V_{DS} = 400\text{ V}$, $V_{GS} = 0\text{ V}$		-	-	25	μA
		$V_{DS} = 320\text{ V}$, $V_{GS} = 0\text{ V}$, $T_J = 125\text{ }^{\circ}\text{C}$		-	-	250	
Drain-source on-state resistance	$R_{DS(on)}$	$V_{GS} = 10\text{ V}$	$I_D = 6.0\text{ A}^b$	-	-	0.55	Ω
Forward transconductance	g_{fs}	$V_{DS} = 50\text{ V}$, $I_D = 6.0\text{ A}^b$		5.8	-	-	S
Dynamic							
Input capacitance	C_{iss}	$V_{GS} = 0\text{ V}$, $V_{DS} = 25\text{ V}$, $f = 1.0\text{ MHz}$, see fig. 5		-	1400	-	pF
Output capacitance	C_{oss}			-	330	-	
Reverse transfer capacitance	C_{rss}			-	120	-	
Total gate charge	Q_g	$V_{GS} = 10\text{ V}$	$I_D = 10\text{ A}$, $V_{DS} = 320\text{ V}$, see fig. 6 and 13 ^b	-	-	63	nC
Gate-source charge	Q_{gs}			-	-	9.0	
Gate-drain charge	Q_{gd}			-	-	32	
Turn-on delay time	$t_{d(on)}$	$V_{DD} = 200\text{ V}$, $I_D = 10\text{ A}$ $R_g = 9.1\text{ }\Omega$, $R_D = 20\text{ }\Omega$, see fig. 10 ^b		-	14	-	ns
Rise time	t_r			-	27	-	
Turn-off delay time	$t_{d(off)}$			-	50	-	
Fall time	t_f			-	24	-	
Gate input resistance	R_g	f = 1 MHz, open drain		0.8	-	5.9	Ω
Internal drain inductance	L_D	Between lead, 6 mm (0.25") from package and center of die contact 		-	4.5	-	nH
Internal source inductance	L_S			-	7.5	-	
Drain-Source Body Diode Characteristics							
Continuous source-drain diode current	I_S	MOSFET symbol showing the integral reverse p - n junction diode 		-	-	10	A
Pulsed diode forward current ^a	I_{SM}			-	-	40	
Body diode voltage	V_{SD}	$T_J = 25\text{ }^{\circ}\text{C}$, $I_S = 10\text{ A}$, $V_{GS} = 0\text{ V}^b$		-	-	2.0	V
Body diode reverse recovery time	t_{rr}	$T_J = 25\text{ }^{\circ}\text{C}$, $I_F = 10\text{ A}$, $dI/dt = 100\text{ A}/\mu\text{s}^b$		-	370	790	ns
Body diode reverse recovery charge	Q_{rr}			-	3.8	8.2	μC
Forward turn-on time	t_{on}	Intrinsic turn-on time is negligible (turn-on is dominated by L_S and L_D)					

Notes

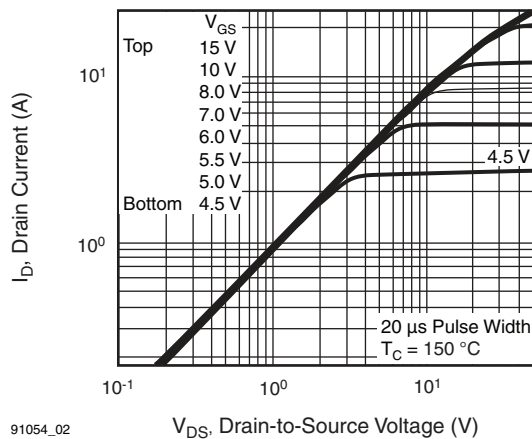
- a. Repetitive rating; pulse width limited by maximum junction temperature (see fig. 11)
b. Pulse width $\leq 300\text{ }\mu\text{s}$; duty cycle $\leq 2\%$

TYPICAL CHARACTERISTICS (25 °C, unless otherwise noted)


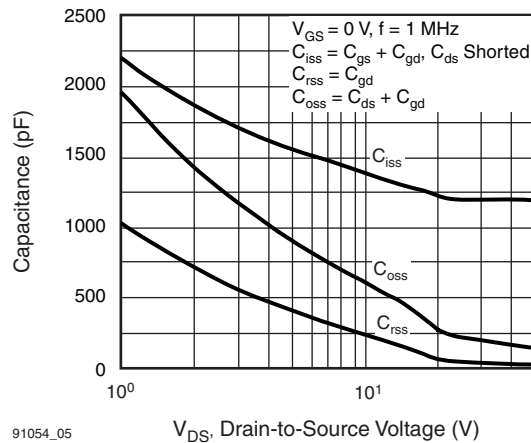
91054_01

Fig. 1 - Typical Output Characteristics, $T_C = 25\text{ }^\circ\text{C}$


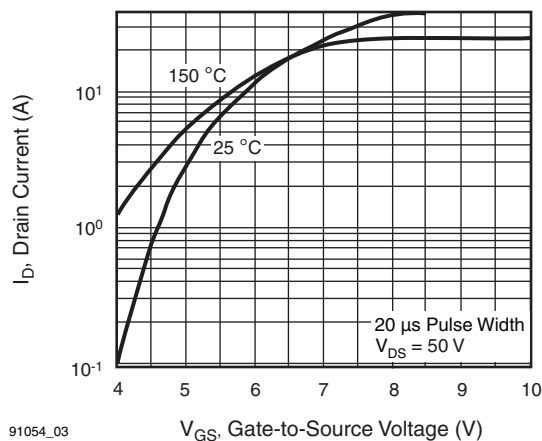
91054_04

Fig. 4 - Normalized On-Resistance vs. Temperature


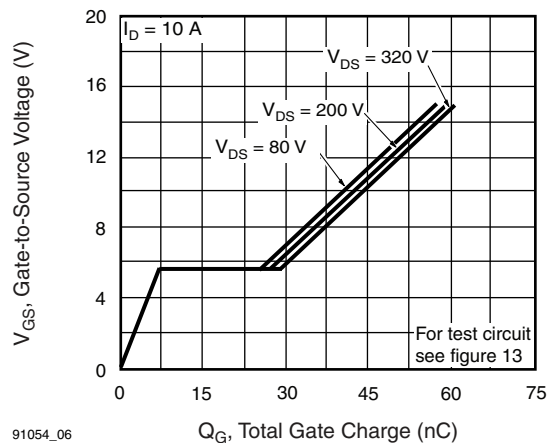
91054_02

Fig. 2 - Typical Output Characteristics, $T_C = 150\text{ }^\circ\text{C}$


91054_05

Fig. 5 - Typical Capacitance vs. Drain-to-Source Voltage


91054_03

Fig. 3 - Typical Transfer Characteristics


91054_06

Fig. 6 - Typical Gate Charge vs. Drain-to-Source Voltage

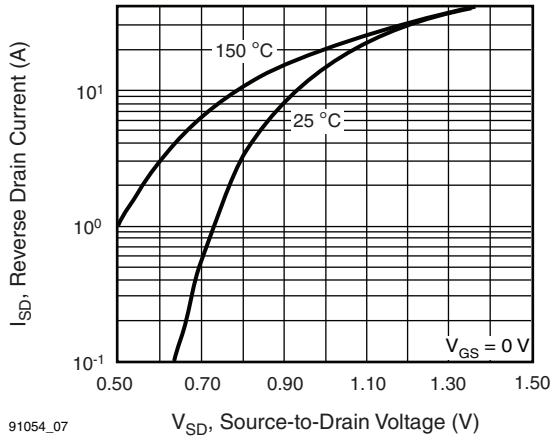
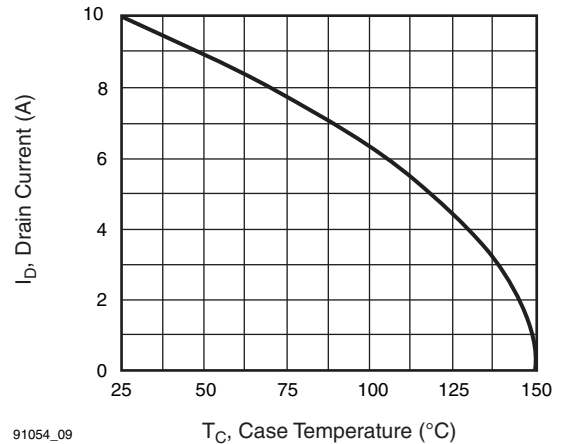
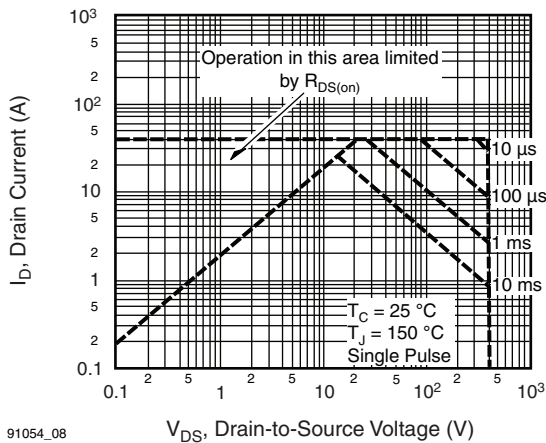
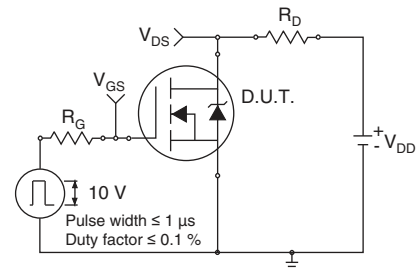
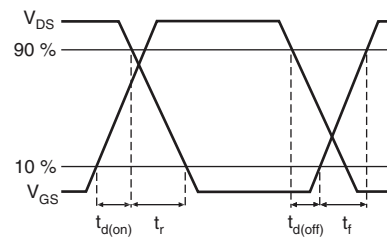
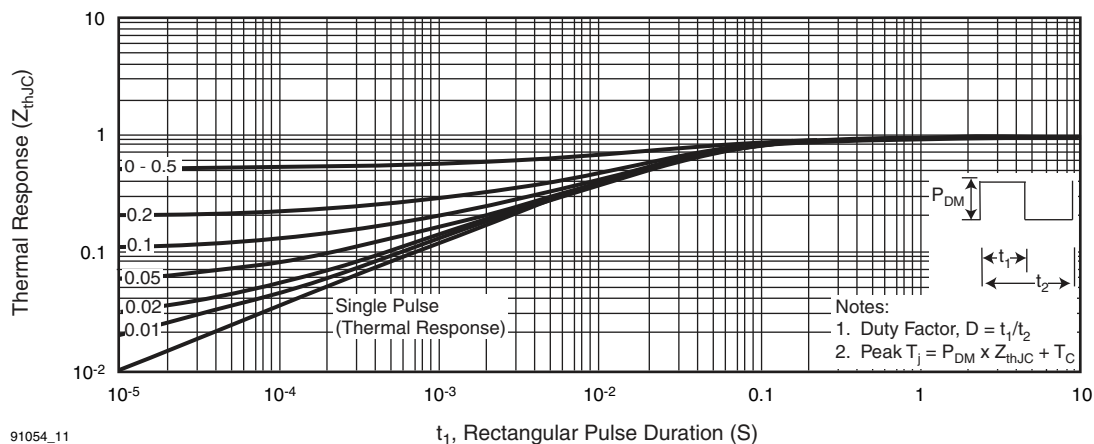
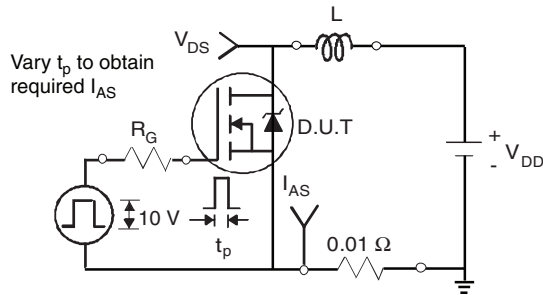
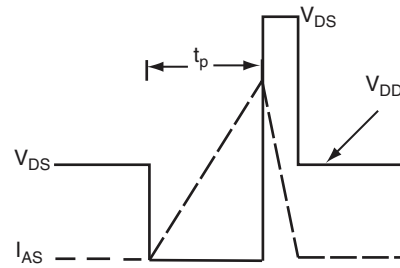
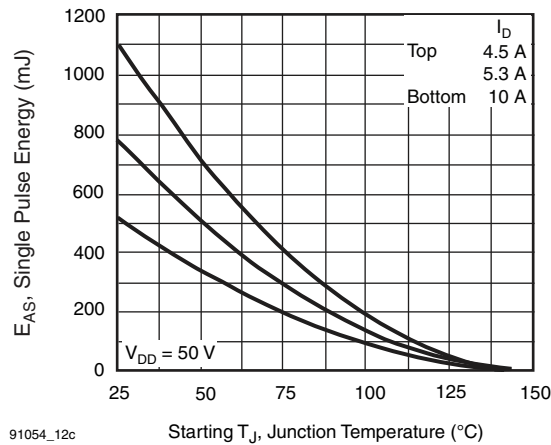
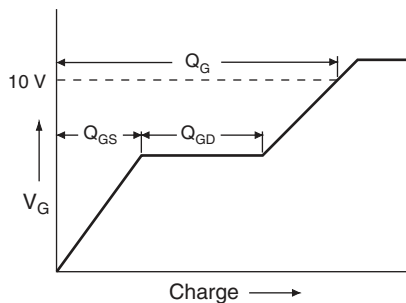
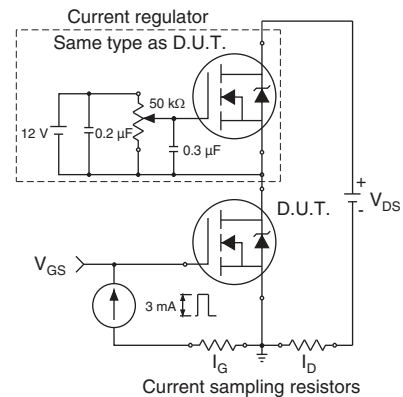
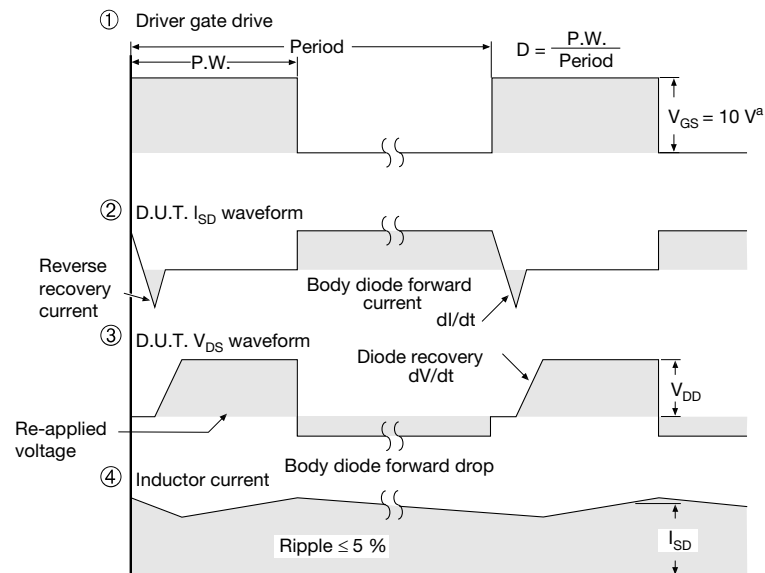
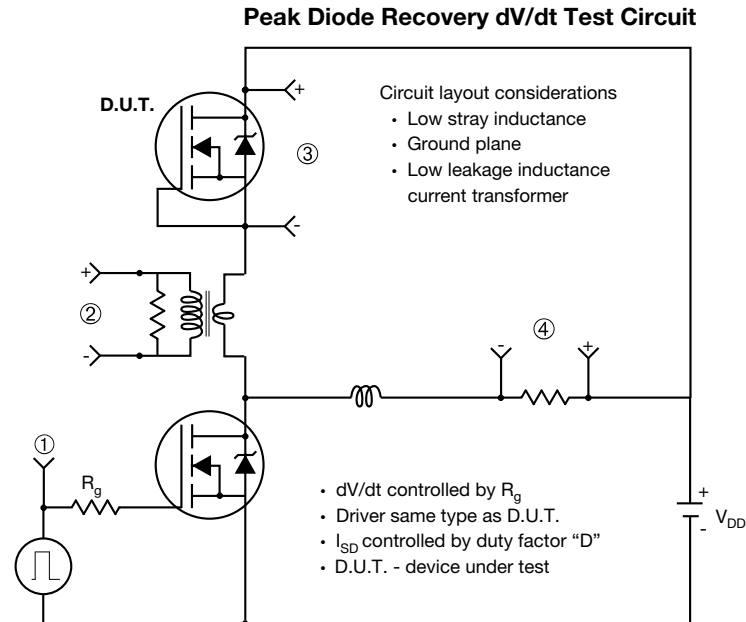

Fig. 7 - Typical Source-Drain Diode Forward Voltage

Fig. 9 - Maximum Drain Current vs. Case Temperature

Fig. 8 - Maximum Safe Operating Area

Fig. 10a - Switching Time Test Circuit

Fig. 10b - Switching Time Waveforms


Fig. 11 - Maximum Effective Transient Thermal Impedance, Junction-to-Case

Fig. 12a - Unclamped Inductive Test Circuit

Fig. 12b - Unclamped Inductive Waveforms

Fig. 12c - Maximum Avalanche Energy vs. Drain Current

Fig. 13a - Basic Gate Charge Waveform

Fig. 13b - Gate Charge Test Circuit

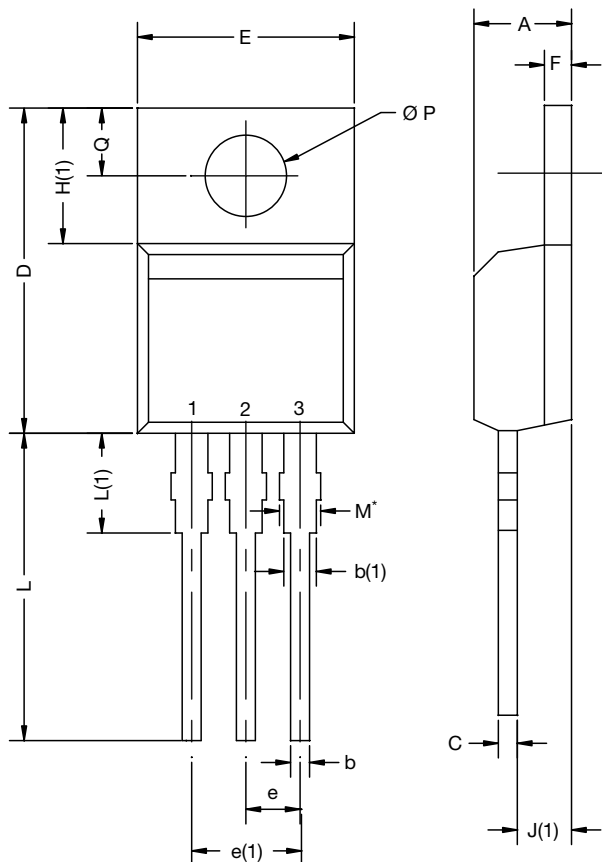

Note

a. $V_{GS} = 5\text{ V}$ for logic level devices

Fig. 14 - For N-Channel

Vishay Siliconix maintains worldwide manufacturing capability. Products may be manufactured at one of several qualified locations. Reliability data for Silicon Technology and Package Reliability represent a composite of all qualified locations. For related documents such as package/tape drawings, part marking, and reliability data, see www.vishay.com/ppg?91054.

TO-220-1

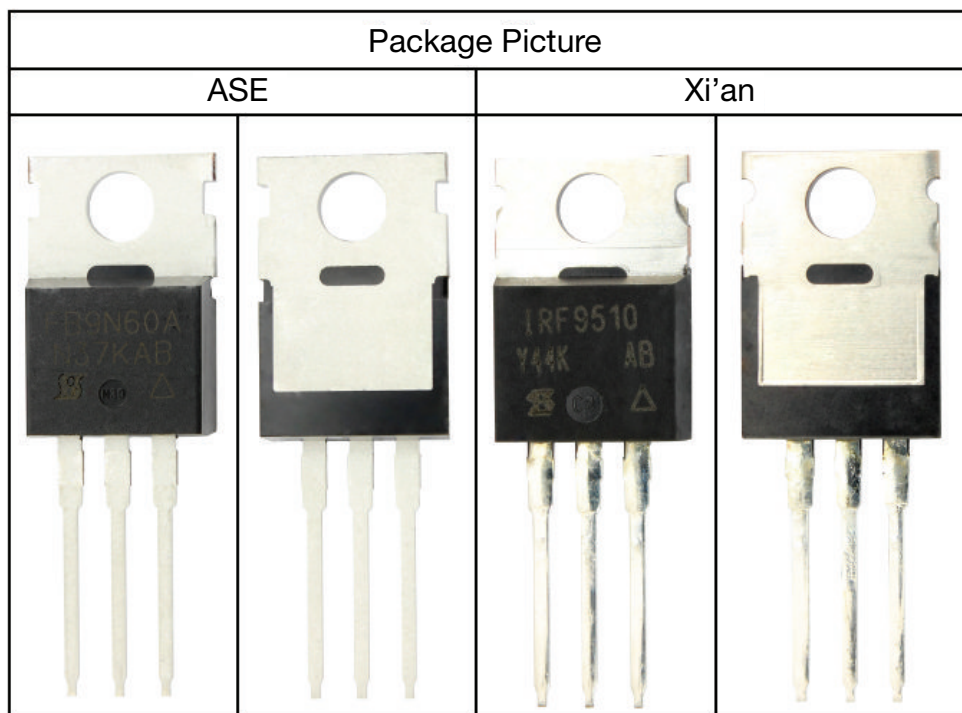


DIM.	MILLIMETERS		INCHES	
	MIN.	MAX.	MIN.	MAX.
A	4.24	4.65	0.167	0.183
b	0.69	1.02	0.027	0.040
b(1)	1.14	1.78	0.045	0.070
c	0.36	0.61	0.014	0.024
D	14.33	15.85	0.564	0.624
E	9.96	10.52	0.392	0.414
e	2.41	2.67	0.095	0.105
e(1)	4.88	5.28	0.192	0.208
F	1.14	1.40	0.045	0.055
H(1)	6.10	6.71	0.240	0.264
J(1)	2.41	2.92	0.095	0.115
L	13.36	14.40	0.526	0.567
L(1)	3.33	4.04	0.131	0.159
$\varnothing P$	3.53	3.94	0.139	0.155
Q	2.54	3.00	0.100	0.118

ECN: X15-0364-Rev. C, 14-Dec-15
DWG: 6031

Note

- M* = 0.052 inches to 0.064 inches (dimension including protrusion), heatsink hole for HVM





Disclaimer

ALL PRODUCT, PRODUCT SPECIFICATIONS AND DATA ARE SUBJECT TO CHANGE WITHOUT NOTICE TO IMPROVE RELIABILITY, FUNCTION OR DESIGN OR OTHERWISE.

Vishay Intertechnology, Inc., its affiliates, agents, and employees, and all persons acting on its or their behalf (collectively, "Vishay"), disclaim any and all liability for any errors, inaccuracies or incompleteness contained in any datasheet or in any other disclosure relating to any product.

Vishay makes no warranty, representation or guarantee regarding the suitability of the products for any particular purpose or the continuing production of any product. To the maximum extent permitted by applicable law, Vishay disclaims (i) any and all liability arising out of the application or use of any product, (ii) any and all liability, including without limitation special, consequential or incidental damages, and (iii) any and all implied warranties, including warranties of fitness for particular purpose, non-infringement and merchantability.

Statements regarding the suitability of products for certain types of applications are based on Vishay's knowledge of typical requirements that are often placed on Vishay products in generic applications. Such statements are not binding statements about the suitability of products for a particular application. It is the customer's responsibility to validate that a particular product with the properties described in the product specification is suitable for use in a particular application. Parameters provided in datasheets and / or specifications may vary in different applications and performance may vary over time. All operating parameters, including typical parameters, must be validated for each customer application by the customer's technical experts. Product specifications do not expand or otherwise modify Vishay's terms and conditions of purchase, including but not limited to the warranty expressed therein.

Hyperlinks included in this datasheet may direct users to third-party websites. These links are provided as a convenience and for informational purposes only. Inclusion of these hyperlinks does not constitute an endorsement or an approval by Vishay of any of the products, services or opinions of the corporation, organization or individual associated with the third-party website. Vishay disclaims any and all liability and bears no responsibility for the accuracy, legality or content of the third-party website or for that of subsequent links.

Except as expressly indicated in writing, Vishay products are not designed for use in medical, life-saving, or life-sustaining applications or for any other application in which the failure of the Vishay product could result in personal injury or death. Customers using or selling Vishay products not expressly indicated for use in such applications do so at their own risk. Please contact authorized Vishay personnel to obtain written terms and conditions regarding products designed for such applications.

No license, express or implied, by estoppel or otherwise, to any intellectual property rights is granted by this document or by any conduct of Vishay. Product names and markings noted herein may be trademarks of their respective owners.